

HIERARCHICAL STELLAR STRUCTURES IN THE LOCAL GROUP DWARF GALAXY NGC 6822

DIMITRIOS A. GOULIERMIS

Max Planck Institute for Astronomy, Königstuhl 17, 69117 Heidelberg, Germany; dgoulier@mpia-hd.mpg.de

STEFAN SCHMEJA, RALF S. KLESSEN¹

Zentrum für Astronomie der Universität Heidelberg, Institut für Theoretische Astrophysik,
Albert-Ueberle-Str. 2, 69120 Heidelberg, Germany;
sschmeja@ita.uni-heidelberg.de; rklessen@ita.uni-heidelberg.de

W. J. G. DE BLOK

University of Cape Town, Private Bag X3, Rondebosch 7701, South Africa;
edeblok@ast.uct.ac.za

AND

FABIAN WALTER

Max Planck Institute for Astronomy, Königstuhl 17, 69117 Heidelberg, Germany;
walter@mpia-hd.mpg.de

Accepted for publication in the Astrophysical Journal

ABSTRACT

We present a comprehensive study of the star cluster population and the hierarchical structure in the clustering of blue stars with ages $\lesssim 500$ Myr in the Local Group dwarf irregular galaxy NGC 6822. Our observational material comprises the most complete optical stellar catalog of the galaxy from imaging with the Suprime-Cam at the 8.2-m SUBARU Telescope. We identify 47 distinct star clusters with the application of the *nearest-neighbor density* method to this catalog for a detection threshold of 3σ above the average stellar density. The size distribution of the detected clusters can be very well approximated by a Gaussian with a peak at ~ 68 pc. The total stellar masses of the clusters are estimated by extrapolating the cumulative observed stellar mass function of all clusters to be in the range $10^3 - 10^4 M_{\odot}$. Their number distribution is fitted very well by a power-law with index $\alpha \sim 1.5 \pm 0.7$, which is consistent with the cluster mass functions of other Local Group galaxies and the *cluster initial mass function*.

The application of the *nearest-neighbor density* method for various density thresholds, other than 3σ , enabled the identification of stellar concentrations in various length-scales, in addition to the detected star clusters of the galaxy. The stellar density maps constructed with this technique provide a direct proof of hierarchically structured stellar concentrations in NGC 6822, in the sense that smaller dense stellar concentrations are located *inside* larger and looser ones. We illustrate this hierarchy by the so-called *dendrogram*, or structure tree of the detected stellar structures, which demonstrates that most of the detected structures split up into several sub-structures over at least three levels. We quantify the hierarchy of these structures with the use of the *minimum spanning tree* method. We find that structures detected at 1, 2, and 3σ density thresholds are hierarchically constructed with a fractal dimension of $D \approx 1.8$. Some of the larger stellar concentrations, particularly in the northern part of the central star-forming portion of the galaxy, coincide with IR-bright complexes previously identified with *Spitzer* and associated with high column density neutral gas, indicating structures that currently form stars. The morphological hierarchy in stellar clustering, which we observe in NGC 6822 resembles that of the turbulent interstellar matter, suggesting that turbulence on pc- and kpc-scales has been probably the major agent that regulated clustered star formation in NGC 6822.

Subject headings: galaxies: dwarf — galaxies: individual (NGC 6822) — galaxies: irregular — galaxies: star clusters — open clusters and associations: general

1. INTRODUCTION

Star formation in galaxies is observed on a wide range of scales, from stellar complexes and aggregates over OB associations to compact embedded clusters, which again often show substructure. These systems are not distinct, independent entities but rather appear to form a continuous hierarchy of structures over all these scales (e.g. Efremov & Elmegreen 1998; Elmegreen et al. 2000). The interstellar matter (ISM) also shows a hierarchical structure

from the largest giant molecular clouds down to individual clumps and cores. The complex hierarchical structure of the ISM is believed to be shaped by supersonic turbulence (e.g., Ballesteros-Paredes et al. 2007). The scaling relations observed in molecular clouds (Larson 1981) can be explained by the effect of turbulence, where energy is injected at very large scales and cascades down to the smallest scales, creating eddies and leading to a clumpy, filamentary structure on all scales. These structures appear self-similar and are therefore often described as fractal. Turbulence is believed to play a major role in star formation by creating density enhancements that become gravitationally unstable and collapse to

¹ Kavli Institute for Particle Astrophysics and Cosmology, Stanford University, Menlo Park, CA 94025, USA

form stars. The spatial distribution of young stars and star clusters probably reflects this process.

There are only few cases, where the formation of stellar structures in star-forming galaxies with resolvable stars can be studied in the complete extent of the galaxy. NGC 6822 is one of these rare galaxies, because it is far enough from us for its whole extent to be fairly covered in small fields-of-view, but also close enough for its bright stellar content to be sufficiently resolved. NGC 6822 (IC 4895) is a Local Group dwarf irregular of type Ir IV-V (van den Bergh 2000). It is the closest dwarf irregular apart from the Magellanic Clouds (MCs), located at a distance of 490 ± 40 kpc from us (Mateo 1998), and belongs to an extended cloud of irregulars named the ‘‘Local Group Cloud’’. Due to its close distance NGC 6822 appears quite extended on the sky; its optical angular diameter is over a quarter of a degree, while its HI disk measures close to a degree (de Blok & Walter 2000). NGC 6822 is relatively near the Galactic plane ($b = -18.4^\circ$) and therefore suffers from significant foreground extinction from the Milky Way (MW). Massey et al. (2007) using multi-band imaging of NGC 6822 within the *Survey of Local Group Galaxies Currently Forming Stars*, derived a total interstellar reddening of $E(B-V) = 0.25 \pm 0.02$, with $E(B-V) = 0.22$ being Galactic. Other recent optical studies of the stellar content of the galaxy (de Blok & Walter 2003; Battinelli et al. 2003) show that NGC 6822 has an extended stellar distribution, with the young blue stars following the distribution of the HI disk (Komiya et al. 2003), while the old and intermediate-age stellar population is found significantly more extended than the HI disk (de Blok & Walter 2006).

The stellar and gas components of NGC 6822 could not explain the shape of the high-resolution rotation curve obtained with the ATCA, except of the very inner regions (Weldrake et al. 2003), and therefore it is considered to be very dark-matter-dominated. NGC 6822 is a metal-poor, relatively gas-rich galaxy with ISM metal abundance of about $0.2 Z_\odot$, i.e. the total fraction of metals is $Z \simeq 0.004$ (Skillman et al. 1989), and total HI mass of $\sim 1.3 \times 10^8 M_\odot$ (de Blok & Walter 2000). Its star formation rate (SFR), based on H α and far-IR fluxes, is found to be around $\sim 0.06 M_\odot \text{yr}^{-1}$ (Mateo 1998; Israel et al. 1996) or $\sim 0.01 M_\odot \text{yr}^{-1}$ (Hunter & Elmegreen 2004). Evidence for increased star formation between 75 and 100 Myr ago is found by Hodge (1980), while Gallart et al. (1996a) found that the star formation in NGC 6822 increased by a factor of 2 to 6 between 100 and 200 Myr ago. Moreover, HST imaging showed that the recent SFR is spatially variable in the central parts of NGC 6822 (Wyder 2001). All these findings are consistent with the mostly constant but stochastic recent star formation histories often derived for other dwarf irregular galaxies (see, e.g., Weisz et al. 2008).

NGC 6822, like most dwarf irregulars, provides an ideal laboratory for the study of galaxy evolution, and in particular at early stages, since its low metallicity and rich gas content suggest that NGC 6822 is still in an early stage of its conversion from gas into stars. Moreover, its relatively simple structure, without dominant spiral arms or bulge, makes the study of the various physical processes related to star formation relatively straightforward. The scope of the present study is the comprehensive understanding of the structural behavior of star formation during the period of the last ~ 500 Myr over the whole extent of NGC 6822. Specifically, we investigate the cluster population of the galaxy in terms of the size, mass

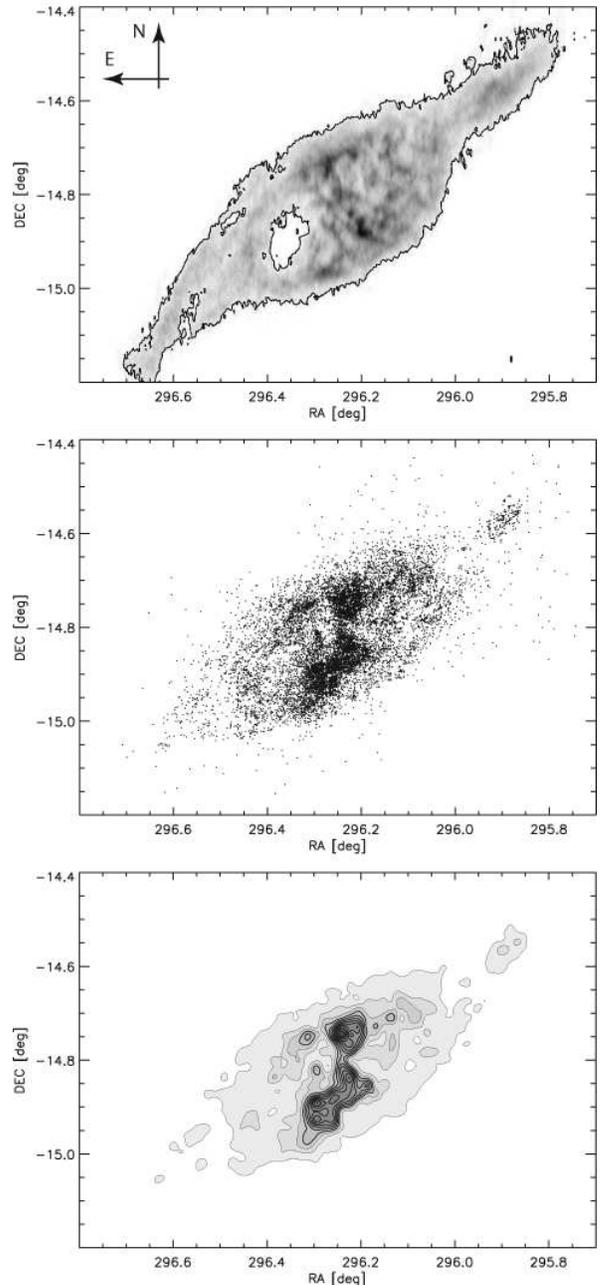


FIG. 1.— Three views of NGC 6822. *Top:* Integrated ATCA HI column density or zeroth-moment map of NGC 6822. The contour indicates the edge of the HI disk of the galaxy at $5 \times 10^{20} \text{ cm}^{-2}$. The grayscale levels run up to $4.3 \times 10^{21} \text{ cm}^{-2}$ (black), which is the maximum column density occurring in this map. The beam of $42''4 \times 12''0$ is indicated in the bottom right. This column density map is adapted from dBW06, for additional representations see Weldrake et al. (2003). *Middle:* Spatial distribution of the blue stars with $B-R \leq 0.5$ on the sky. This distribution highlights the concentration of the blue stars with ages $\lesssim 500$ Myr in the inner parts of the galaxy, and the general extent of these stars in a disk-like structure, similar to the HI disk of the galaxy. *Bottom:* Number density map of the blue stars shown in the middle panel, measured in $64'' \times 64''$ boxes. The iso-density contour levels run from the mean background density in steps of 1σ , σ being the standard deviation of the background density. Isoleths of density $\geq 5\sigma$ are plotted with thicker lines.

and structural characteristics of the detected stellar systems. We also study the clustering behavior of stars and its relation to hierarchically structured stellar concentrations within the whole extent of NGC 6822.

A comprehensive study of the star complexes, i.e., large-scale star-forming regions with sizes of the order of few hundreds pc, was recently presented by Karamelas et al. (2009). These authors provide a complete catalog of star complexes in NGC 6822, their positions and sizes, based on the data collected within the *Survey of Local Group Galaxies Currently Forming Stars* (SLGGCFS; Massey et al. 2006, 2007). This study is limited to the brightest stars of the galaxy with $B \lesssim 22.5$ due to the detection limit of the SLGGCFS and only to its central part, which is covered by the survey. In our investigation here we extend the study of the spatial distribution of young stars and hierarchical star formation in NGC 6822 to the smallest detectable structures, and to the complete extent of the galaxy, including the potentially tidal systems, with the use of original photometric material that comprises a stellar sample 6 times larger than that used by Karamelas et al. (2009). Our catalog extends to fainter magnitudes by $B \simeq 2.5$ mag on the main sequence, and covers the whole area of the HI disk of the galaxy (Fig. 1 top). As a consequence, in the present study we investigate star formation in a wider range of lengthscales, covering structures with sizes from few tens pc (clusters and small associations) to few hundreds pc (stellar aggregates and complexes). Apart from the study of hierarchy, our detection method allows us to also address important issues of star formation, such as the structural behavior of the clusters in NGC 6822 and the *cluster mass function* of the galaxy.

The observational material, which includes the most complete stellar sample observed in NGC 6822 (de Blok & Walter 2006, from here on dBW06) is described in § 2. In § 3 we define the stellar content of the galaxy for the purpose of our study and select the type of stars our analysis focuses on. We identify the clusters of the galaxy with the application of the *nearest neighbor* (from here on NN) method in § 4, and we discuss their sizes and masses in § 5. In § 6 we construct the *cluster mass function* of NGC 6822, and compare our results with those of other galaxies. The structural parameters of the detected clusters are measured and cross-correlated in § 7. The hierarchical behavior in the spatial distribution of the blue stellar content of NGC 6822 is investigated in § 8, with the detection of stellar structures in various length-scales larger than typical clusters, and the construction of their *denrogram*, to determine the degree of hierarchical clustering. We discuss our results concerning hierarchy in § 9. Finally, we summarize the findings of this study in § 10.

2. OBSERVATIONAL MATERIAL

2.1. Photometric Stellar Catalog

In this investigation we use the photometric data derived from images of NGC 6822 taken with Suprime-Cam on the 8.2-m SUBARU Telescope at Mauna Kea, Hawaii. Suprime-Cam consists of 5×2 CCDs of 2048×4096 pixels each, providing a total field of view of $34' \times 27'$ with a $0''.2$ pixel size (Miyazaki et al. 2002). We make use of the results based on two sets of archival Suprime-Cam images observed in B , R and I . The first set consists of two *deep* pointings, covering the whole of the HI disk of NGC 6822 (see Fig. 1 top). It was observed on 2001 October 15 and 19, and it is described in detail by Komiyama et al. (2003). The second set of images was taken in 2000 June, during the early days of Suprime-Cam, and it consists of a single *shallow* pointing toward the optical center of NGC 6822. dBW06 stress the importance of the combination of the deep photometry with the

shallow for a complete understanding of the stellar population of NGC 6822, due to the high light gathering power of SUBARU, which saturates stars down to quite faint magnitudes. The present study is based on the comprehensive photometric analysis of both data sets performed earlier in dBW06 for the investigation of the stellar content of NGC 6822. As a consequence, much of the information provided in this section comes from the results of these authors. We repeat it here for reasons of completion.

2.2. Color-Magnitude Diagram

In the present study we utilize the final merged photometric catalog of stellar sources derived in dBW06 by combining the catalogs of stars detected in both deep and shallow exposures. This catalog contains 250 237 stellar sources identified in all three B , R , I wavelengths. In our analysis we limit ourselves to only those “high-quality” objects with a photometric uncertainty $\sigma \leq 0.1$ mag in all three bands, constraining the stellar catalog to 208 894 members. The B , $B-R$ color-magnitude diagram (CMD) of these stars is shown in Fig. 2. This CMD has a larger dynamic range than those derived from previous investigations (Komiyama et al. 2003; Battinelli et al. 2003; de Blok & Walter 2003), and that of SLGGCFS (Massey et al. 2006, 2007), probing to fainter magnitudes. By adding in the shallow data our stellar sample also covers the O- and B-type star regime of NGC 6822, and consequently it is the ideal stellar sample for the investigation of the most recent clustered star formation in this galaxy.

3. YOUNG STELLAR POPULATIONS IN NGC 6822

The CMD of Fig. 2 contains a mixture of different stellar populations. A complete discussion on all observed stellar types in NGC 6822 is given by dBW06. In short this CMD shows three important distinct components: (i) The vertical “blue plume” centered on $B-R \sim 0.3$, which consists mostly of young stars in NGC 6822. (ii) The red population of stars covering the area of the CMD with $1 \lesssim B-R \lesssim 1.75$ and $m_B \gtrsim 23$ (named the “red-tangle” by Gallart et al. 1996b), which contains mainly the old and intermediate-age stellar content of NGC 6822 with ages between 1 and 10 Gyr. (iii) A vertical band around $B-R \sim 1.5$, which consists of contaminant Galactic foreground stars (see also Massey et al. 2007). Also clearly identified as being due to foreground stars is the region with $2 \lesssim B-R \lesssim 3$ and $m_B \gtrsim 24.5$ (dBW06).

For our study we focus on the blue populations, and therefore we select our stellar sample from the “blue plume”. This area in the CMD with $B-R < 0.75$ consists mostly of young main-sequence (MS) and more evolved helium-burning blue loop (BL) stars down to an age of roughly 0.5 Gyr. In the absence of variable foreground extinction as found toward NGC 6822, MS stars would occupy the blue side of the plume and BL stars the red. Therefore, since we are interested in the youngest observed populations, we constrain our selection of stars to those with $B-R \leq 0.5$, which correspond to ages roughly $\lesssim 500$ Myr, according to the Padova evolutionary models (Girardi et al. 2002).

Fig. 1 (middle) shows the spatial distribution of the selected sample of blue stars with $B-R \leq 0.5$. Since the final photometric catalog of dBW06 is the combined shallow photometric catalog in the inner part with the deep catalog in the outer part of the galaxy, these authors checked the outer field for saturated stars that should have been incorporated in an equivalent shallow catalog of the outer field. They found that there

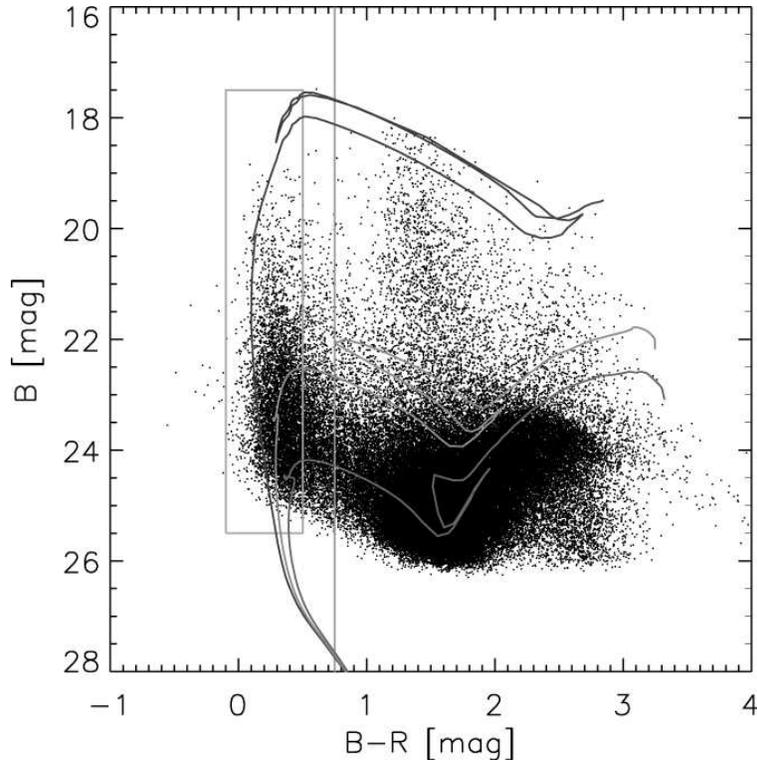


FIG. 2.— $B-R$, R CMD of all 208 894 stars detected with good photometry in the observed SUBARU fields of NGC 6822. Indicative isochrones for 20 (blue), 200 (orange) and 500 Myr (red) from the Padova evolutionary grid of models (Girardi et al. 2002) are overlaid for a nominal metallicity $Z = 0.004$ (Skillman et al. 1989), reddening $E(B-V) = 0.25$ (Massey et al. 2007) and distance modulus $m-M = 23.53$ (Gallart et al. 1996a). The green vertical line sets the limits of the “blue plume” stars, and the light blue box signifies the CMD area of the MS stars with $(B-R) \leq 0.5$, selected in this study for the identification of young stellar structures with ages down to roughly 500 Myr (see text in § 3). [Color version of the figure will be available in the published electronic version of the paper.]

are very few saturated stars present, and therefore the stellar distribution shown in the middle panel of Fig. 1 represents very well the whole observed blue stellar sample, despite the lack of a shallow photometry for the outer field. The corresponding surface density distribution of the blue MS stars constructed by simple star counts in a smoothed grid of elements $64'' \times 64''$ in size is shown in the bottom panel of Fig. 1.

From the maps of Fig. 1 one may conclude that the young blue stars (i) are distributed across the whole HI disk, apart maybe from its southeastern part, (ii) they are mostly concentrated in the central part of the galaxy in a “S-like” feature, and (iii) their distribution is rather clumpy. It should be noted that the density contour map of Fig. 1 (bottom) is a smoothed visualization of the large-scale stellar structures that exist in NGC 6822. The application, later, of the NN method (§ 4) allows a far more detailed identification of the smallest possible stellar concentrations of the galaxy.

Interestingly, the star counts of Fig. 1 revealed as an *independent* stellar structure the so-called “Northwestern Cloud”, located at a position (R.A., Decl.) $\approx (295.9, -14.6)$, which is speculated to be a separate system that is *currently interacting* with the main body of NGC 6822 and is thought to be responsible for the tidal arms in the southeast of the galaxy (de Blok & Walter 2000, 2003). It could also have triggered the star formation that eventually led to the creation of the large hole in the southeastern part of the main HI disk, centered at a position (R.A., Decl.) $\approx (296.35, -14.9)$ (dBW06).

The stellar content of the Cloud is dominated by a well-defined blue MS, and there are two low-brightness HII regions identified in the Cloud (dBW06). Both findings indicate that the Cloud has experienced recent star formation. Unfortu-

nately, the shallow SUBARU images do not cover its area, and therefore only stars up to $m_B \sim 20.5$ are measured, the brightest and bluest of which being well described by a $\log \tau \sim 7$ Padova isochrone. The presence, however, of a few saturated stars clustered in the same way as the unsaturated ones and the $H\alpha$ observations suggest that even younger stars may be present in the Northwestern Cloud (dBW06).

4. DETECTION OF CONCENTRATIONS OF YOUNG STARS

The blue MS population selected in the previous section for the study of clustered star formation within the last ~ 500 Myr comprises 13 727 stars. In this section we apply the nearest neighbor (NN) method to investigate *how these stars are clustered*. A short introduction of the method, which is described by, e.g., Schmeja et al. (2009), is given below (§ 4.1). Our method enables the detection of dense stellar concentrations, revealing the most prominent *cluster population* of NGC 6822 (§ 4.2). While these systems span an order of magnitude in physical dimensions, we refer to all of them as *clusters*, although this term in principle applies only to a specific small-scale single-age class of systems, and not to the whole distribution of detected objects. Independent repetitions of the method, for different density thresholds (§ 8), revealed less dense stellar concentrations systematically belonging to larger ones, providing evidence of hierarchy in the distribution of the blue MS stars in NGC 6822. We refer to all these concentrations generally as *structures*.

4.1. The Nearest Neighbor Density Method

Star clusters are usually identified as regions of a certain overdensity with respect to the background stellar density. The NN method, introduced by Casertano & Hut (1985)

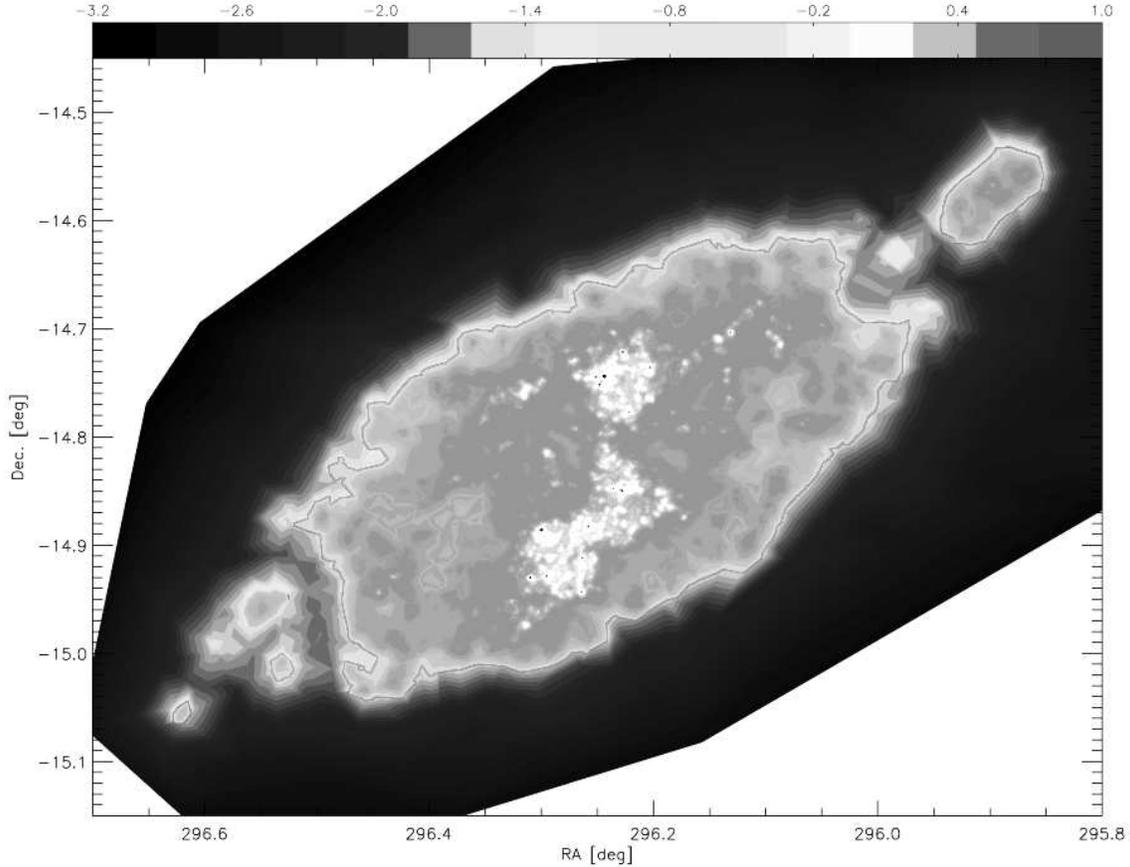


FIG. 3.— The stellar density map of NGC 6822 (in logarithmic scale), constructed with the NN density method applied to stars with ages $\lesssim 500$ Myr for the 10th NN. All stellar concentrations detected with density higher than 3σ above the average background are identified as members of the cluster population of NGC 6822. [Color version of the figure will be available in the published electronic version of the paper.]

based on earlier work by von Hoerner (1963), estimates the local source density ρ_j by measuring the distance from each object to its j th nearest neighbor:

$$\rho_j = \frac{j-1}{S(r_j)} m \quad (1)$$

where r_j is the distance of a star to its j th nearest neighbor, $S(r_j)$ the surface area with the radius r_j and m the average mass of the sources ($m = 1$ when considering number densities). The chosen value of j depends on the sample size, and is correlated with the sensitivity to the density fluctuations being mapped. A small j value increases the locality of the density measurements while increasing the sensitivity to random density fluctuations. On the other hand a large j value will reduce that sensitivity at the cost of some locality.

The positions of the cluster centers are defined as the density-weighted enhancement centers (Casertano & Hut 1985):

$$x_{d,j} = \frac{\sum_i x_i \rho_j^i}{\sum_i \rho_j^i}, \quad (2)$$

where x_i is the position vector of the i th cluster member and ρ_j^i the j th NN density around this object. Similarly, the density radius $r_{d,j}$ is defined as the density-weighted average of the distance of each star from the density center:

$$r_{d,j} = \frac{\sum_i |x_i - x_{d,j}| \rho_j^i}{\sum_i \rho_j^i}. \quad (3)$$

This radius typically corresponds to the core radius of the cluster (Casertano & Hut 1985).

We applied the NN method to our data considering several values for the nearest neighbors (j). Casertano & Hut (1985) have shown that low j values, in particular $j = 1$ or 2 , are extremely sensitive to statistical fluctuations, therefore they suggest using a value of $j \geq 6$. On the other hand, the choice of a too large j value results in a loss of sensitivity to real density variations on smaller scales. Monte Carlo simulations have shown that a value of $j = 20$ is adequate to the detection of clusters with about 10 to 1500 members (B. Ferreira, private communication). However, since we aim at the detection of clusters even poorer than 10 members, we applied several test runs of the method that showed that $j = 10$ is a reasonable choice of number of NN.

The 10th NN density map of the blue MS stars in NGC 6822 is shown in Fig. 3. This map demonstrates that the selected blue MS stars are distributed in almost the whole extent of the disk of the galaxy and the northern-western cloud, as it has been demonstrated by the iso-density contour map of Fig. 1. The NN density map, however, along with the general (average) stellar distribution of these stars throughout the galaxy, can also track in detail individual stellar concentrations. Specifically, while the low-density distribution of the blue MS stars, shown in blue and green scales, clearly outlines the disk of NGC 6822 and the north-western cloud, the high-density levels (shown in yellow and red) show a more clumpy and centrally concentrated stellar distribution, reveal-

ing individual stellar systems as density peaks.

4.2. Detected Young Clusters

A reasonable density level, above which the detected density enhancements are accepted as star clusters is 3σ above the average density, where σ is the standard deviation of the background density. As a consequence, the original list of detected objects comprises all stellar density enhancements with density peaks at and above the 3σ threshold. However, since our method does not set any dimensional limit for the detected objects, this list includes the smallest density peaks that could be possibly identified. Indeed, the smallest objects in the list are found to be minute density peaks, which include only one or two stars, and therefore they are most probably spurious detections at the level of the noise. Naturally, these detections cannot be related to real physical stellar concentrations, but rather to the background density fluctuations. As a consequence, we exclude them from the final catalog of detected young clusters in NGC 6822, which thus comprises all stellar concentrations of 3 or more stellar members, that are found with our method to have 10th NN density values 3σ above the average density.

The detected clusters contain MS stars in the whole observed magnitude range of $B \lesssim 25$. However, the range of brightness of the majority of the stars included in every cluster can be used to assign an indicative maximum age to each of them. We divided, thus, the observed catalog of MS stars into four magnitude ranges and we again computed the corresponding 10th NN density and applied a 3σ threshold for the detection of clusters. Each of the selected magnitude ranges corresponds to a specific range of stellar ages, with the older age, specified by the *turn-off* of the best-fitting isochrone, being associated to the faint magnitude limit. The four magnitude ranges were selected to include almost equal number of stars so that each run of the method would have the same statistical significance. We assign this age-limit to each of the stellar sub-catalogs with the use of the evolutionary models of Girardi et al. (2002) for the distance, metallicity and reddening of NGC 6822, by applying isochrone fitting of the CMD. In this manner we are able to have a direct estimate of the age-range of the clusters identified in the corresponding stellar sub-catalogs, with those detected in the whole catalog having the oldest observable age of ~ 500 Myr.

Although we cannot have an estimate of the actual age of each cluster, this approach is important for two reasons. First, age determination of the detected clusters by isochrone fitting of their individual CMDs is not really possible, due to their poor stellar number statistics. Moreover, the derivation of ages from integrated surface brightness of each cluster would require the application of population synthesis techniques, which would introduce important model-dependent uncertainties, again due to low stellar numbers, especially for the faint clusters. The selected magnitude ranges are $B < 21$, $B < 22$, $B < 23$ and $B \geq 23$, which according to the models correspond to maximum ages for the clusters of $\tau_{\max} \simeq 95$, 150, 250 and 500 Myr respectively. The majority of the detected clusters (36) are found to comprise stars in the faintest ranges or in the whole magnitude range and therefore $\tau_{\max} \simeq 500$ Myr is assigned to them. Seven clusters are found with $\tau_{\max} \simeq 250$ Myr, one with $\tau_{\max} \simeq 150$ Myr, and three with $\tau_{\max} \simeq 95$ Myr. The maximum ages of the clusters are given in column 4 of Table 3 for comparison to their dynamical timescales derived in § 7. In the following Section we discuss in detail the characteristics of the detected clusters.

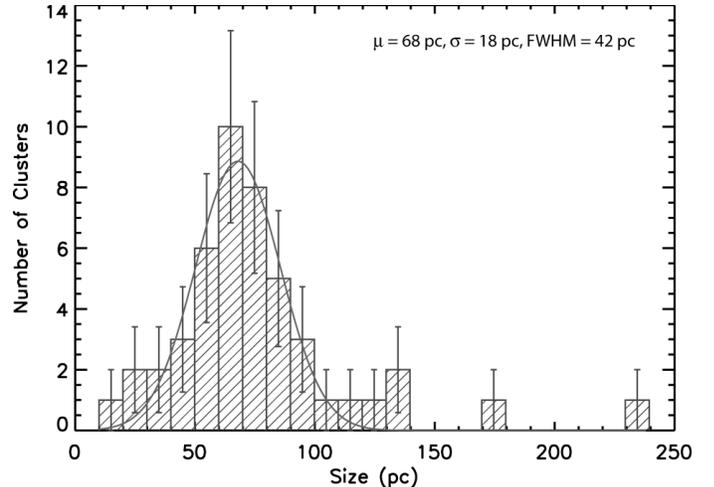


FIG. 4.— Histogram of the size distribution of detected young star clusters in NGC 6822, with a bin size of 10 pc. Parameters of the best-fit Gaussian (red line) are also given. [Color version of the figure will be available in the published electronic version of the paper.]

5. THE CLUSTER POPULATION OF NGC 6822

The catalog of identified star clusters in NGC 6822 consists of 47 clusters, the physical dimensions of which are defined by the 3σ density level in the 10th NN density map. Table 1 lists the identified clusters with the positions of their 10th NN density centers (Columns 2 and 3), the number of cluster members (Column 4), and their density and limiting radii (Columns 5 and 6 respectively) in seconds of an arc. The *density radius*, r_{dens} , (Column 5) is derived from the NN method and Eq. (3) and roughly corresponds to the core radius of each system. The so-called *effective radius* (e.g., Carpenter 2000) or *equivalent radius* (e.g., Román-Zúñiga et al. 2008) of the systems (Columns 6 and 7) is the radius of a circle with the same area as the area enclosed by the cluster-defining 3σ contour ($r_{\text{equiv}} = \sqrt{A_{\text{cl}}/\pi}$). The total *expected* number of stars, N , (Column 10) and mass, M_{cl} , (Column 11) are estimated from the extrapolation of the mass spectrum of each cluster assuming that it reassembles the average Galactic IMF (see § 5.2).

5.1. Size Distribution of the Clusters

From Table 1 it can be seen that our catalog of young clusters covers a variety of systems, starting with those of the minimum of 3 stellar members with dimensions $\lesssim 20$ pc (cluster 47), up to those with maximum size of almost 240 pc, including 77 stars (cluster 1). The size distribution of the clusters constructed by binning them according to their dimensions is shown in Fig. 4. Dimensions are given in physical units (pc) assuming a distance modulus of $m-M = 23.53$. A functional fit to this histogram shows that the size distribution of the detected clusters can be very well approximated by a normal distribution. According to the best-fit Gaussian, drawn with a red line in Fig. 4, the dimensions of the detected systems are clustered around an average of $\simeq 68$ pc with a standard deviation of $\simeq 18$ pc. This is a rather interesting result, considering that, as pointed out earlier by various authors (e.g., Efremov et al. 1987; Ivanov 1996; Gouliermis et al. 2003), young stellar associations *in different galaxies* seem to have typical dimensions close to this value (between 65 and 93 pc) with an average of 80 pc. If, however, this length-scale is characteristic for star formation is still under debate (see, e.g., Bastian et al. 2007; Gouliermis 2010).

TABLE 1
THE CLUSTER POPULATION OF NGC 6822 WITH AGES $\lesssim 500$ MYR, DETECTED WITH 10TH NN DENSITY
VALUES 3σ ABOVE BACKGROUND.

Cluster ID	R.A. (deg)	Decl. (deg)	n_*	r_{dens} (")	r_{equiv} (")	(pc)	B_{br} (mag)	m_{max} (M_{\odot})	N	M_{cl} ($10^3 M_{\odot}$)
1	296.24692	-14.74281	77	14.70	50.29	119.47	19.34	17.42	87812	9.99 ± 0.68
2	296.22754	-14.84399	47	10.24	37.68	89.50	18.94	19.33	62032	7.06 ± 0.49
3	296.26373	-14.91980	29	7.60	29.18	69.32	20.35	13.23	47708	5.43 ± 0.38
4	296.25827	-14.87879	24	7.09	29.02	68.93	19.37	17.27	48364	5.50 ± 0.39
5	296.29990	-14.88262	24	4.42	25.76	61.20	21.19	10.36	29269	3.33 ± 0.23
6	296.29492	-14.92559	19	5.50	24.38	57.91	22.38	7.17	34399	3.91 ± 0.28
7	296.28711	-14.89010	15	7.31	21.20	50.37	21.89	8.37	12538	1.43 ± 0.10
8	296.26413	-14.93961	15	3.74	20.20	47.99	21.52	9.37	34797	3.96 ± 0.29
9	296.22186	-14.77319	14	4.04	20.10	47.76	20.19	13.82	19757	2.25 ± 0.16
10	296.20294	-14.73244	16	3.84	19.99	47.48	19.30	17.58	16055	1.83 ± 0.13
11	296.23712	-14.72879	14	4.39	18.20	43.23	20.25	13.61	16998	1.93 ± 0.14
12	296.29254	-14.88720	11	4.26	17.64	41.90	21.92	8.29	18219	2.07 ± 0.15
13	296.28781	-14.93673	10	6.29	17.31	41.12	20.03	14.46	26106	2.97 ± 0.22
14	296.23611	-14.84454	10	2.81	17.24	40.94	21.49	9.46	21508	2.45 ± 0.18
15	296.31003	-14.92668	12	2.13	17.20	40.86	22.16	7.68	25761	2.93 ± 0.22
16	296.24265	-14.75290	10	2.99	16.30	38.73	20.82	11.55	21005	2.39 ± 0.17
17	296.29214	-14.90718	13	5.14	16.17	38.40	21.69	8.89	10096	1.15 ± 0.08
18	296.22964	-14.73439	10	6.30	16.01	38.03	20.95	11.14	10703	1.22 ± 0.08
19	296.22729	-14.71831	11	1.67	16.01	38.03	21.43	9.64	22769	2.59 ± 0.19
20	296.27225	-14.88502	10	3.15	15.72	37.34	21.09	10.67	34637	3.94 ± 0.30
21	296.21454	-14.76024	10	4.29	15.47	36.75	21.23	10.25	22983	2.61 ± 0.19
22	296.23825	-14.73670	9	4.81	15.46	36.73	20.75	11.80	12147	1.38 ± 0.10
23	296.26706	-14.92909	7	3.51	15.27	36.28	20.81	11.60	20109	2.29 ± 0.17
24	296.26959	-14.87903	9	4.01	14.69	34.89	22.70	6.45	14426	1.64 ± 0.12
25	296.21567	-14.84455	8	4.55	14.26	33.88	21.36	9.85	31207	3.55 ± 0.27
26	296.13132	-14.69955	11	2.95	14.06	33.39	19.58	16.35	38558	4.39 ± 0.35
27	296.26364	-14.90800	8	2.39	13.98	33.22	21.55	9.30	29133	3.31 ± 0.26
28	296.27594	-14.92400	7	4.27	13.55	32.18	21.59	9.18	9849	1.12 ± 0.08
29	296.22586	-14.77637	7	3.80	13.03	30.95	20.43	12.94	25421	2.89 ± 0.22
30	296.27118	-14.89139	7	3.03	12.82	30.46	23.03	5.79	17718	2.01 ± 0.15
31	296.26489	-14.87163	4	1.76	12.80	30.42	20.93	11.20	11498	1.31 ± 0.09
32	296.22665	-14.87727	9	2.60	12.79	30.38	21.38	9.79	26342	3.00 ± 0.23
33	296.22006	-14.84672	6	2.38	12.67	30.09	22.24	7.50	31063	3.53 ± 0.28
34	296.22711	-14.72315	8	2.98	12.33	29.30	20.86	11.41	26343	3.00 ± 0.23
35	296.20230	-14.76187	6	4.90	11.71	27.81	20.88	11.37	13942	1.59 ± 0.12
36	296.19022	-14.85646	7	2.68	11.49	27.29	19.84	15.22	18638	2.12 ± 0.16
37	296.31396	-14.97089	5	2.49	11.33	26.90	21.46	9.55	15824	1.80 ± 0.14
38	296.20490	-14.75966	5	2.06	11.11	26.40	21.70	8.88	9558	1.09 ± 0.08
39	296.23492	-14.72453	6	2.86	10.97	26.06	20.87	11.38	12427	1.41 ± 0.11
40	296.23090	-14.75460	6	2.81	10.37	24.64	20.92	11.22	17777	2.02 ± 0.16
41	296.23541	-14.73430	4	2.33	9.63	22.87	22.36	7.21	10157	1.15 ± 0.09
42	296.19272	-14.86216	3	2.43	9.00	21.39	22.82	6.22	12311	1.40 ± 0.11
43	296.24420	-14.73231	4	1.62	8.27	19.65	22.86	6.13	13818	1.57 ± 0.12
44	296.31229	-14.75217	4	1.99	7.41	17.59	21.29	10.05	11492	1.31 ± 0.10
45	296.25198	-14.88950	4	2.42	5.78	13.74	22.49	6.91	20460	2.32 ± 0.20
46	296.24365	-14.87206	3	2.52	5.58	13.25	21.42	9.66	14739	1.68 ± 0.14
47	296.21973	-14.88315	3	4.02	3.85	9.14	22.18	7.65	8670	0.99 ± 0.09

NOTE. — A detailed description of the parameters is given in § 5.

5.2. Masses of the Clusters

The sample of detected clusters naturally includes a variety of systems not only concerning their physical dimensions but also their stellar content and in consequence their total mass. While our data are not deep enough to cover the whole extent of masses for the stellar members of the detected clusters, and not complete enough to provide us with the actual numbers of stars (per luminosity or mass range) for each of them, it is worthwhile to perform a first-order calculation of the total stellar mass included in each detected cluster, based on several assumptions. We identify the number of stars included in each cluster and their luminosities from our photometric catalog. Then, in order to have a first estimation of the total mass of each cluster we (i) build the observed Luminosity Function (LF) of each cluster, (ii) apply a mass-luminosity relation (M-LR) based on the stellar evolutionary models for the conversion of this LF to the Mass Function (MF) of the cluster,

and (iii) extrapolate this observed MF to the lower masses for the calculation of the total mass of each cluster.

5.2.1. Mass-Luminosity Relation

For the establishment of the conversion of stellar luminosities to masses, we use the evolutionary models by Girardi et al. (2002). Our clusters identification is applied for all detected stars of NGC 6822 formed within the last ~ 500 Myr, and therefore the identified clusters are expected to have different ages from each other within this time range. As a consequence, in order to construct a realistic M-LR for each cluster, one should establish a correct age with the use of the CMD of the detected stars in the cluster. However, the construction of individual M-LR for each cluster is not possible, because in all cases the stellar numbers found within the detected clusters are not sufficient to build complete and informative CMDs.

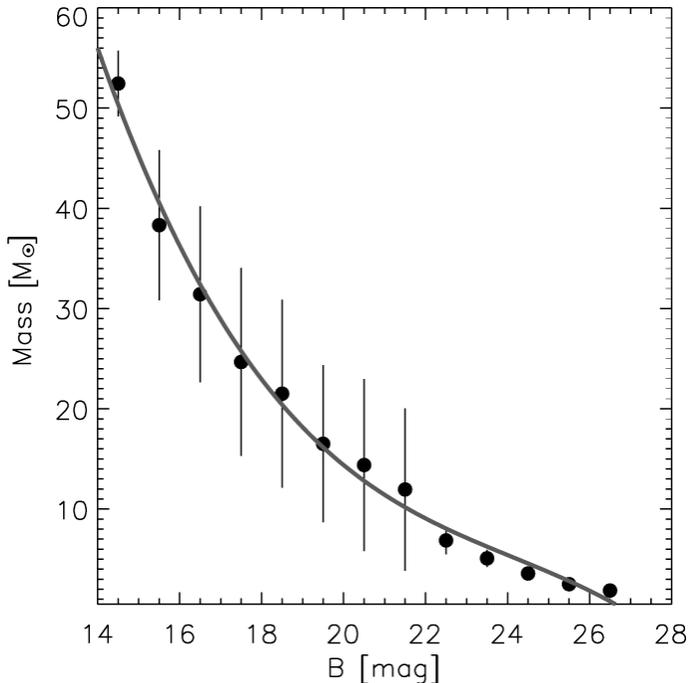


FIG. 5.— Mass-Luminosity relation constructed with the use of isochrones from the grid of evolutionary models by Girardi et al. (2002) for the metallicity and at the distance of NGC 6822. Isochrones of a large variety in ages are used for the correct quantification of the uncertainties in the determination of the cluster masses due to age differences among the identified clusters. [Color version of the figure will be available in the published electronic version of the paper.]

On the other hand, one may construct a *global* M-LR to be used for the conversion of LFs to MFs for *all* clusters, but this M-LR should be established from evolutionary models that cover a large range in ages. Indeed, as it is seen in the CMD of Fig. 2 the observed MS is populated by stars in an increasingly larger variety of ages towards fainter magnitudes down to $B \simeq 25$ mag. Therefore, we construct a *global* M-LR for all identified clusters using the evolutionary models of Girardi et al. (2002) not for specific ages, but for all available ages and for the appropriate metallicity of $Z = 0.004$. With this treatment the uncertainties in stellar masses due to the age differences among the identified clusters will be inherited to the global M-LR and affect accordingly the determination of the total mass of the clusters. The derived M-LR, for an assumed average reddening $E(B-V) = 0.25$ (Massey et al. 2007) and distance modulus $m-M = 23.53$ (Gallart et al. 1996a), is shown in Fig. 5. From this figure it can be seen that indeed the stellar mass uncertainty is a function of the MS magnitude, with the larger uncertainties appearing for the parts of the MS where models of different ages show the greatest differences in the derived masses. While $B \simeq 25$ mag corresponds more or less to our detection limit, and our stellar sample does not include stars brighter than $B \simeq 17.5$ mag, we construct our M-LR for a more extended magnitude range for reasons of completeness in its shape. This M-LR is being used for the direct transformation of the luminosity of each star detected within the limits of one of the NGC 6822 clusters into mass.

5.2.2. The Stellar Mass Spectrum of the Clusters

The stellar mass function is the number distribution of stars according to their masses, constructed for a given volume of space in a cluster. This function is known as the stellar *Present Day Mass Function*, which is usually called simply the *Mass*

Function of the cluster. In this study we refer to this function as the *Stellar Mass Function* (SMF), to distinguish it from the *Cluster Mass Function* discussed later. The SMF of a cluster is described by the function $\xi(\log m)$, which gives the number of stars per unit logarithmic (base ten) mass interval $d \log m$ per unit area (e.g. $/\text{kpc}^2$). Alternatively, one may refer to the *Stellar Mass Spectrum* (SMS) of the cluster, $f(m)$, which is the number of stars per unit mass interval dm per unit area. The common use of both these functions is based on the definition of the stellar *Initial Mass Function* (IMF), various forms of which are discussed by, e.g., Kroupa (2002) and Chabrier (2003). All these distributions are usually parametrized by their indices. Specifically, for the SMS $f(m)$, and the SMF $\xi(\log m)$, these indices are defined as

$$\gamma = \frac{d \log f(m)}{d \log m} \quad (4)$$

and

$$\Gamma = \frac{d \log \xi(\log m)}{d \log m}. \quad (5)$$

These two indices are basically the logarithmic derivatives or slopes of $f(m)$ and $\xi(\log m)$ respectively and for power-law distributions they are independent of mass (Scalo 1986). A reference value for the SMF slope is $\Gamma = -1.35$, which is the index of the classical IMF for stars in the solar neighborhood with masses $0.4 \lesssim M/M_{\odot} \lesssim 10$, found by Salpeter (1955). The corresponding SMS index is $\gamma = \Gamma - 1 \simeq -2.35$. For comparison, the lognormal field-star IMF by Miller & Scalo (1979) has $\Gamma \simeq -(1 + \log m)$. A basic relation between SMF and SMS is $\xi(\log m) = (\ln 10) \cdot m \cdot f(m) \simeq 2.3 \cdot mf(m)$ (see Scalo 1986).

The construction of the SMS of each cluster is essential for the calculation of its *expected* total mass through extrapolation of its SMS. However, in most of the cases of identified clusters in NGC 6822 the detected stellar numbers are *not* sufficient for the construction of a meaningful SMS for each cluster. This problem can be surpassed with the use of a common SMS constructed by all stars detected within the identified clusters. This approach, naturally, assumes that the SMS is indeed *universal*, in line with most findings in the local universe (see, e.g., Massey 2006; Bastian et al. 2010). We construct the *global* SMS of the clusters in NGC 6822 by counting all stars detected within the limits of all the 47 identified clusters according to their masses, and distributing the stellar masses in mass-bins $1 M_{\odot}$ wide. This SMS is given in Table 2, and it is shown in Fig. 6. This figure also shows the best-fit line derived from the application of a linear regression to the most complete mass-bins corresponding to masses between ~ 5 and $13 M_{\odot}$.

The determination of the slope of power laws from uniformly binned data using linear regression is found to comprise biases, which are caused by the correlation between the number of stars per bin and the assigned weights (Maíz Apellániz & Úbeda 2005). However, we measured the average mass of the stars counted in each bin for the construction of the global SMS, and we found that it is almost equal to the mean mass of the bin. The corresponding standard deviations per bin, are found to be smaller than $1 M_{\odot}$, the width of each bin, and therefore there is no “leak” of stars expected from one mass-bin to its neighboring, and thus no random fluctuations in the constructed SMS. The *measured* average mass per bin, rather than the mean mass of each bin,

TABLE 2
THE GLOBAL *Stellar Mass Spectrum*
CONSTRUCTED FROM ALL STARS DETECTED
WITHIN THE LIMITS OF THE 47 IDENTIFIED
CLUSTERS IN NGC 6822.

$\langle m_{\text{bin}} \rangle$ M_{\odot}	N_{stars}	$\langle m \rangle$ M_{\odot}	$\sigma_{(m)}$ M_{\odot}	ρ_{*} stars/kpc ² / M_{\odot}
2.50	1	2.94	-	7.43 ± 3.71
3.50	31	3.75	0.03	118.83 ± 20.68
4.50	123	4.51	0.02	460.48 ± 41.19
5.50	124	5.46	0.04	464.19 ± 41.35
6.50	84	6.42	0.01	315.65 ± 34.04
7.50	59	7.35	0.04	222.81 ± 28.52
8.50	45	8.49	0.05	170.82 ± 24.91
9.50	31	9.41	0.04	118.83 ± 20.68
10.50	16	10.50	0.11	63.13 ± 14.85
11.50	15	11.36	0.04	59.42 ± 14.38
12.50	6	12.52	0.17	25.99 ± 9.10

NOTE. — The mean mass per bin, given in Col. 1, is comparable to the measured average mass of Col. 3, calculated from all stars counted per bin, given in Col. 2. The corresponding standard deviations, given in Col. 4, do not exceed the width of each bin ($1 M_{\odot}$). The counted stellar numbers per surface used for the construction of the SMS, and the corresponding Poisson errors are given in Col. 5. Values are plotted in Fig. 6.

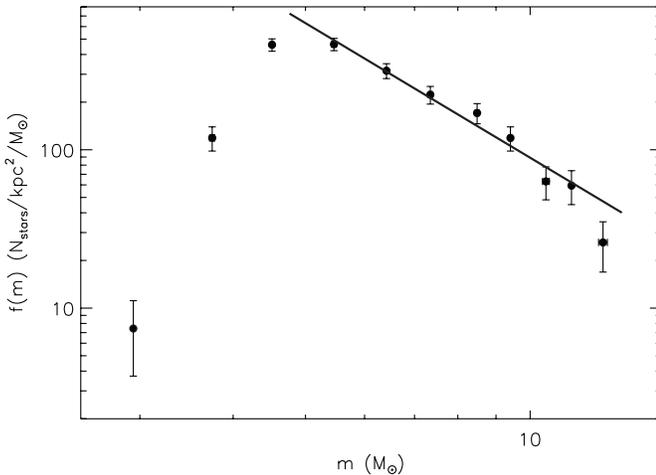


FIG. 6.— The Stellar Mass Spectrum of all stars comprised within the areas covered of all 47 detected clusters with age $\lesssim 500$ Myr in NGC 6822. The total sample includes 561 stars with masses between ~ 3 and $13 M_{\odot}$. The sample is complete for stars down to $\sim 5 - 6 M_{\odot}$. A linear fit (solid line) to the SMS down to this mass limit gives a slope of γ between -2.21 and -2.82 , very close to the typical Galactic field slope for the same mass range. The plotted points correspond to the average mass of all stars counted per mass-bin with the x-axis errors derived from the standard deviation of the masses per bin. The errors on the y-axis reflect the Poisson statistics. See also text in § 5.2.2.

is plotted in Fig. 6, and the corresponding $\sigma_{(m)}$ are shown as error bars on the x-axis, demonstrating the accuracy of the pointing of each mass-bin. The linear regression for the most complete mass range of $5 \lesssim m/M_{\odot} \lesssim 13$ provides a SMS slope γ , which is exceptionally close to the average Galactic field value, equal to -2.5 ± 0.5 (black-solid line in Fig. 6).

5.2.3. Total Masses of the Clusters

An estimate of the total mass of each cluster in NGC 6822 can be achieved through integration of its SMS. However, as we discuss earlier, the construction of a meaningful SMS

for each cluster is not possible due to low stellar numbers, and therefore we make use of the global SMS assuming that this distribution is universal and representative of all clusters. While, according to our assumption, the slope of the SMS should not be different from one cluster to the other, the absolute stellar numbers per mass-bin of the SMS in each cluster are different and thus the corresponding total cluster mass. Indeed, the individual SMS of the clusters do deviate from the global SMS, mostly in stellar numbers and, in some cases of clusters with very few stars, in the slope. This is demonstrated in Fig. 7, where the SMS of seven selected indicative clusters from our sample are plotted. In this figure it can be seen that the general trend of the SMS slope indeed seems consistent with the global SMS (solid line), but the stellar numbers (per surface unit) are quite different. These differences will determine the differences in total mass of the clusters. We estimate the cluster masses in three steps:

- (i) We first extend the observed global SMS to the low-mass regime below our detection limit according to the generally accepted Galactic field mass spectrum. This mass spectrum is usually parametrized with a series of power laws, with exponents changing in different mass ranges (see, e.g., Scalo 1998). The most recent parameterization is that by Kroupa (2002), according to which the slope γ changes from $\gamma = -0.3$ in the substellar mass range, to $\gamma = -1.3$ for masses between $0.08 M_{\odot}$ and $0.5 M_{\odot}$, $\gamma = -2.3$ for $0.5 \leq m/M_{\odot} < 1$, and γ between -2.7 and $-2.3 (\pm 0.3)$ for stars of higher masses. This SMS is generally characterized as the Galactic average, in the sense that it is reasonably valid for different regions of the Galaxy.

Considering that the SMS of all clusters identified in NGC 6822 should have a multi-power law form, with exponents that change at the same mass limits as the Galactic SMS, we assume that the global SMS of the clusters has the average slope of those measured in § 5.2.2, equal to $\gamma = -2.5 \pm 0.5$, for stars with masses down to our completeness limit of about $5.5 M_{\odot}$ and we extrapolate it with the same slope down to the mass limit of $1 M_{\odot}$. For the extrapolation of the global SMS to sub-solar masses we consider the exponents of the Galactic SMS, as they are discussed above for stars with masses down to $\sim 0.1 M_{\odot}$.

The extrapolated global SMS, following the parameterization by Kroupa (2002), is thus a three-part power law function of the form

$$f(m) \propto \left(\frac{m}{m_i} \right)^{\gamma_i} \quad \text{with } i = 1, 2, 3. \quad (6)$$

The slopes γ depending the mass range are

$$\begin{aligned} \gamma_1 &= -1.3 \pm 0.5 & , & \quad 0.1 \leq m/M_{\odot} < 0.5 \\ \gamma_2 &= -2.3 \pm 0.3 & , & \quad 0.5 \leq m/M_{\odot} < 1.0 \\ \gamma_3 &= -2.5 \pm 0.5 & , & \quad 1.0 \leq m/M_{\odot}. \end{aligned} \quad (7)$$

- (ii) We then normalize the extrapolated global SMS to fit the stellar numbers observed in every cluster. Specifically, we normalize the extrapolated global SMS to the mass-bin of around 5 to $6 M_{\odot}$, because all detected clusters, including those with only three stars, show to have at least one star at this specific mass range. Therefore, by normalizing the global SMS to this mass limit

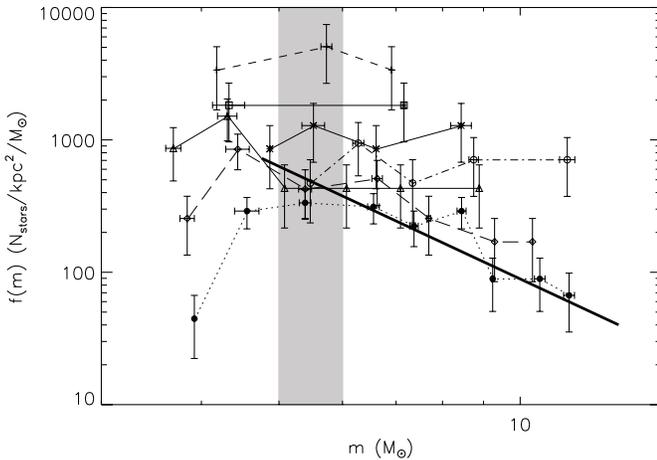


FIG. 7.— Indicative Stellar Mass Spectra (SMS) from the sample of clusters detected in NGC 6822. Different symbols are used for plotting the SMS of seven indicative clusters, comprising a variety of objects from the richest cluster in the sample (Cluster # 1) plotted with filled circles to one of the poorest (Cluster # 41) with only two mass-bins plotted with open boxes. Points for individual clusters are also connected together with lines. The slope of the global SMS is represented by the solid line, as in Fig. 6. This graph demonstrates the variability in stellar numbers among the clusters, and the inability to extrapolate the observed SMS of each cluster, due to low stellar numbers and thus the necessity for the use of a global SMS. The mass range over which the global SMS is considered for extrapolation for all clusters, $m \simeq 5 - 6 M_{\odot}$, is indicated by the vertical shaded area. See also text in § 5.2.3

we apply a comparable approach to all, rich and poor, clusters.

- (iii) We finally integrate the normalized SMS of each cluster from the largest mass observed in the cluster to the smaller stellar mass assumed to exist in all clusters of $0.1 M_{\odot}$, and derive an estimation of the total cluster mass, from its surface stellar density

$$M_{\text{cl}} = \rho_{\star} \pi r_{\text{equiv}}^2, \quad (8)$$

where

$$\rho_{\star} = \int_{0.1}^{m_{\text{max}}} f(m) dm. \quad (9)$$

The total stellar numbers of the clusters derived from this method and the corresponding total stellar masses are given in Table 1 (Cols. 10 and 11 respectively).

6. MASS DISTRIBUTION OF THE CLUSTERS

The total stellar masses of the clusters of NGC 6822, as derived above, cover a range over an order of a magnitude with the smaller cluster mass being around $10^3 M_{\odot}$. The number distribution of the clusters according to their masses, i.e. the mass spectrum of the clusters, which is widely termed the *Cluster Mass Function* (CMF) is shown in logarithmic scale in Fig. 8. The CMF derived from young ($\lesssim 10$ Myr) star clusters is defined as the *Cluster Initial Mass Function* (CIMF). Considering that the CMF follows the functional form of a power-law, as it is generally assumed, we applied a linear regression to the data of Fig. 8. The best fit returns the function

$$\log N_{\text{cl}} = (-1.47 \pm 0.72) \log M_{\text{cl}} + (1.60 \pm 0.31). \quad (10)$$

We found, thus, that the CMF of the massive clusters of NGC 6822 can be described by a power law with index $\sim -1.5 \pm 0.7$.

6.1. Comparison with the CIMF

Previous works on the CIMF in a variety of galactic environments have shown that this function is well described by a power law with index -2 (see, e.g., Gieles 2009):

$$\frac{dN}{dM} \propto M^{-\alpha}, \quad \alpha = 2. \quad (11)$$

Specifically, the CMF of star clusters in the Antennae galaxies (NGC 4038/9) with ages $\lesssim 160$ Myr is found, over the range $10^4 \lesssim M_{\text{cl}}/M_{\odot} \lesssim 10^6$, to have an index of -2 (Zhang & Fall 1999). McCrady & Graham (2007) constructed the CMF of 19 super star clusters (SSCs) with $M_{\text{cl}} > 10^5 M_{\odot}$ and ages of the order of 10 Myr in the nuclear starburst of M 82, and found a power-law with an index -1.91 ± 0.06 . The SSCs with an average age ~ 10 Myr in the nearby starburst galaxies NGC 3310 and NGC 6745 are investigated by de Grijs et al. (2003), who find CMF indexes of -2.04 ± 0.23 and -1.96 ± 0.19 respectively. These CMFs correspond to the CIMF due to the youthfulness of the cluster samples. All three studies on massive star clusters agree to an almost identical CIMF index of -2 . In addition, a similar CIMF index of -2.1 ± 0.3 is found for 10 Myr old clusters in the mass range $2.5 \cdot 10^3 < M_{\text{cl}}/M_{\odot} < 5 \cdot 10^4$ in the inner spiral arms of M 51 (Bik et al. 2003). All the aforementioned studies provide evidence of a “universality” of the CIMF. Since most of the clusters in our sample have undergone substantial dynamical and stellar evolution, their CMF cannot be compared with the CIMF. It is interesting, though, to notice that the derived CMF index of NGC 6822 in the mass range $10^3 - 10^4 M_{\odot}$ of $\sim -1.5 \pm 0.7$ is well within 1σ of the “global” CIMF, as the large uncertainties in our CMF do not allow us to identify any significant difference from it.

6.2. Comparison with the Magellanic Clouds

Our CMF of NGC 6822, which covers stellar concentrations with ages of up to $\tau \simeq 500$ Myr, should have been significantly affected by evolutionary effects and therefore it is not directly comparable to the CIMF. Comparable CMFs in terms of cluster masses and ages to that derived here are those presented by de Grijs & Anders (2006) and de Grijs & Goodwin (2008) for the cluster populations in the Large and Small Magellanic Clouds (LMC, SMC) respectively. The CMF index in the LMC is given as a function of minimum mass and maximum age, based on mass-limited samples (see de Grijs & Anders 2006, their Table 3 and Fig. 8). For $\log(m_{\text{cl}}/M_{\odot})_{\text{min}} = 3$ and $\log(\tau/\text{yr})_{\text{max}} = 8.7$, which corresponds to our sample, de Grijs & Anders (2006) find a CMF index -1.98 ± 0.08 , an average value which is somewhat different than ours, but nevertheless covered by our uncertainties, and quite similar to the CIMF. In addition, in the SMC de Grijs & Goodwin (2008) find a CMF with index $\alpha \lesssim 1.2$ for almost the same cluster mass range with ours. This slope falls within 1σ of our CMF slope, and is therefore also consistent with it.

7. STRUCTURAL PARAMETERS OF THE CLUSTERS

We estimate the stellar density, ρ_{cl} , in the half-mass radius, r_{h} , of each cluster and the disruption time, t_{d} , of the cluster due to interaction with passing-by interstellar clouds, as described in, e.g., Gouliermis et al. (2002, their section 6). The former is calculated assuming spherical symmetry for all clusters as

$$\rho_{\text{cl}} \equiv \frac{M_{\text{cl}}}{\frac{4}{3}\pi r_{\text{h}}^3} \left(\frac{M_{\odot}}{\text{pc}^3} \right), \quad (12)$$

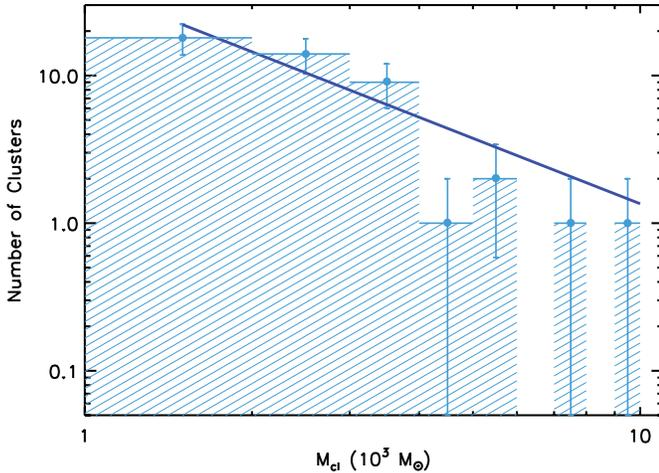


FIG. 8.— The Mass Spectrum of the star clusters or the *Cluster Mass Function* of NGC 6822, based on calculation of their total stellar masses in § 5.2.3 under the assumption that all clusters follow a common high-mass stellar IMF, extrapolated to the sub-stellar limit according to the *Average Galactic IMF*. [Color version of the figure will be available in the published electronic version of the paper.]

while the latter is given as (Spitzer 1958)

$$t_d = 1.9 \times 10^8 \varrho_{cl} \text{ (years)}. \quad (13)$$

The dynamical status of a young star cluster is defined by two additional time-scales, the *crossing* and the *two-body relaxation* time, which are given as (e.g., Kroupa 2008)

$$t_{cr} \equiv \frac{2r_h}{\sigma} \quad \text{and} \quad t_{relax} = 0.1 \frac{N}{\ln N} t_{cr} \quad (14)$$

respectively. The three-dimensional velocity dispersion of the stars in the cluster, σ , is given as

$$\sigma = \sqrt{\frac{GM_{cl}}{\epsilon r_h}}, \quad (15)$$

where ϵ is the star formation efficiency (SFE) and r_h the half-mass radius of the cluster. We estimate these time-scales for the clusters of our sample, with the application of Eqs. (14), assuming the same SFE with several nearby Galactic gas-embedded clusters, which has been found to range typically from 10% to 30% (Lada & Lada 2003). In our calculations we assume an average value of $\epsilon \simeq 0.2$, which leads to values of σ between 12 and 89 km s⁻¹ for our clusters.

For the measurement of the r_h of each cluster we estimate the so-called *Spitzer* radius, r_{Sp} . Considering that $r_h \simeq 0.9 r_{Sp}$ only for dynamically relaxed spherical clusters (e.g., Spitzer 1969), we can only approximate the actual r_h of our clusters. The Spitzer radius is a dynamically stable radius, defined by the mean-square distance of the stars from the center of the cluster (e.g., Spitzer 1987) as

$$r_{Sp} \equiv \sqrt{\frac{\sum_{i=1}^N r_i^2}{N}}, \quad (16)$$

where r_i is the projected radial distance of the i th star of the cluster in a total sample of N stars. We estimate this radius for each cluster in our sample only from the stars identified within its limits, for which there are positions available, and not from the expected total number of stars according to the extrapolated mass spectrum of each cluster. As a consequence, the accuracy of the derived r_{Sp} of each cluster is subject to the number of its identified stars.

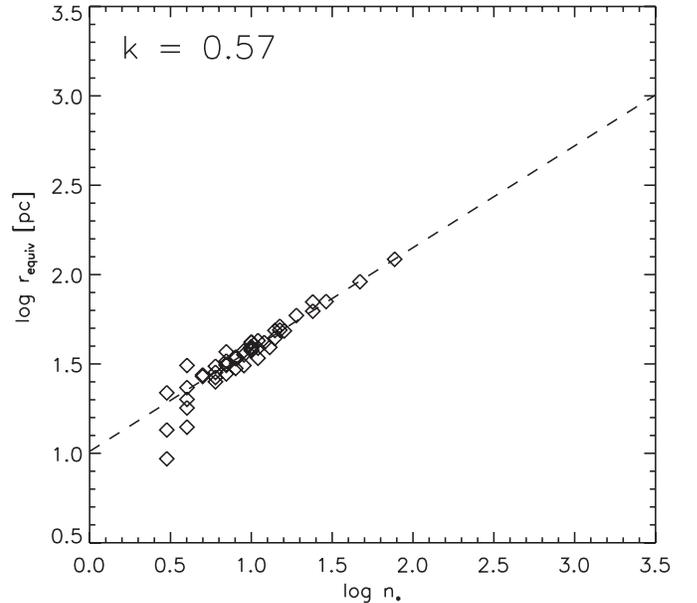


FIG. 9.— Correlation between the number of detected stars and r_{equiv} for the cluster population of NGC 6822 (10th NN, 3σ density detection level). This correlation is consistent with that found for Galactic embedded clusters (see § 7.1).

The estimation of r_{Sp} allows the evaluation of σ and ϱ_{cl} of the clusters and consequently of their t_d , t_{cr} and t_{relax} according to equations (13) and (14). For the latter we use the *expected* total number of stellar members, N , as it is derived from the extrapolation of the mass spectrum of each cluster. All additional estimated structural parameters for the young clusters of NGC 6822 are provided also in Table 3.

7.1. Parameters correlations of the clusters in NGC 6822

A correlation between the number of stars in a cluster and the radius of the cluster has been found in Galactic embedded clusters (Adams et al. 2006; Allen et al. 2007): While n_* and r vary by about two orders of magnitude, the average surface density of cluster members ($n_*/\pi r^2$) is nearly constant. We find the same correlation, following a power law, between n_* and r_{equiv} for the clusters identified in NGC 6822, which span an even wider range in radius, n_* , and age (Fig. 9). The correlation has a slope in the log-log plot of $k \simeq 0.6$, comparable to that found by Adams et al. (2006) for their sample of young Galactic clusters. Our fit, which has a correlation coefficient of $q \approx 0.92$, is affected by the smallest clusters ($n_* \leq 5$) that show some scatter. A similar correlation exists also between n_* and r_{dens} , but it becomes less clear when using the expected number of stars N instead of the observed number n_* . A correlation between number of stars and radius is also observed for the stellar structures we identify below with the application of the NN method with density levels different than 3σ (see § 8.4).

8. HIERARCHICAL CLUSTERING IN NGC 6822

The majority of stars form in clusters and aggregates of various sizes and masses (Lada & Lada 2003; Allen et al. 2007). Young star clusters are often found inside larger complexes, which can be parts of even larger structures. In turn, stellar clusters often consist of distinct subclusters, appearing to form a hierarchy of systems over a wide range of scales (e.g. Efremov & Elmegreen 1998; Elmegreen et al. 2000). The ISM is also hierarchically structured (sometimes

TABLE 3
STRUCTURAL PARAMETERS OF THE STAR CLUSTERS OF NGC 6822.

Cluster ID	R.A. (deg)	Decl. (deg)	τ_{\max} (Myr)	ϱ_{cl} (M_{\odot}/pc^3)	r_{Sp} (pc)	σ (km s^{-1})	t_{d} (Myr)	t_{cr} (Myr)	t_{relax} (Myr)
1	296.24692	-14.74281	500	0.05 ± 0.00	36.92	89.0	9.00	0.81	626.83
2	296.22754	-14.84399	500	0.09 ± 0.01	26.87	63.8	16.49	0.82	463.66
3	296.26373	-14.91980	500	0.14 ± 0.01	21.16	49.7	25.97	0.83	369.59
4	296.25827	-14.87879	500	0.11 ± 0.01	22.79	51.9	21.07	0.86	385.82
5	296.29990	-14.88262	500	0.33 ± 0.02	13.48	31.1	61.66	0.85	242.05
6	296.29492	-14.92559	500	0.21 ± 0.02	16.40	37.1	40.14	0.87	285.19
7	296.28711	-14.89010	500	0.05 ± 0.00	18.43	23.8	10.32	1.52	201.97
8	296.26413	-14.93961	500	0.63 ± 0.05	11.42	31.2	120.41	0.72	238.97
9	296.22186	-14.77319	500	0.39 ± 0.03	11.11	23.2	74.29	0.94	187.72
10	296.20294	-14.73244	150	0.30 ± 0.02	11.28	21.0	57.75	1.05	174.13
11	296.23712	-14.72879	250	0.25 ± 0.02	12.31	22.6	47.05	1.07	186.06
12	296.29254	-14.88720	500	0.32 ± 0.02	11.54	22.7	61.08	1.00	185.32
13	296.28781	-14.93673	500	0.18 ± 0.01	15.92	31.9	33.31	0.98	251.41
14	296.23611	-14.84454	250	1.25 ± 0.09	7.76	20.2	237.77	0.75	162.28
15	296.31003	-14.92668	500	2.16 ± 0.16	6.87	20.8	410.02	0.65	164.18
16	296.24265	-14.75290	250	0.97 ± 0.07	8.37	20.7	184.95	0.79	166.92
17	296.29214	-14.90718	500	0.07 ± 0.01	15.45	19.5	14.13	1.55	169.78
18	296.22964	-14.73439	95	0.06 ± 0.00	16.53	20.8	12.23	1.56	179.65
19	296.22729	-14.71831	500	3.48 ± 0.26	5.62	17.7	660.40	0.62	141.35
20	296.27225	-14.88502	500	1.44 ± 0.11	8.67	27.1	273.73	0.63	207.82
21	296.21454	-14.76024	500	0.36 ± 0.03	11.97	25.9	69.20	0.90	206.96
22	296.23825	-14.73670	500	0.14 ± 0.01	13.46	20.0	25.71	1.32	170.37
23	296.26706	-14.92909	95	0.71 ± 0.05	9.15	21.2	135.34	0.85	171.56
24	296.26959	-14.87903	500	0.30 ± 0.02	10.94	19.6	56.74	1.09	164.55
25	296.21567	-14.84455	500	0.41 ± 0.03	12.76	31.2	77.53	0.80	241.65
26	296.13132	-14.69955	500	2.19 ± 0.17	7.82	27.2	416.40	0.56	206.02
27	296.26364	-14.90800	500	2.36 ± 0.18	6.94	22.2	449.03	0.61	173.41
28	296.27594	-14.92400	500	0.23 ± 0.02	10.50	15.9	43.85	1.29	138.64
29	296.22586	-14.77637	500	0.72 ± 0.06	9.88	24.8	136.12	0.78	195.75
30	296.27118	-14.89139	500	0.93 ± 0.07	8.03	18.6	176.13	0.84	153.02
31	296.26489	-14.87163	500	2.88 ± 0.21	4.77	11.6	548.05	0.81	99.22
32	296.22665	-14.87727	250	2.23 ± 0.17	6.84	21.0	424.44	0.64	165.29
33	296.22006	-14.84672	500	3.21 ± 0.25	6.40	22.0	610.64	0.57	170.91
34	296.22711	-14.72315	500	1.56 ± 0.12	7.72	22.3	295.83	0.68	175.53
35	296.20230	-14.76187	250	0.20 ± 0.02	12.45	20.6	37.25	1.18	173.04
36	296.19022	-14.85646	500	1.49 ± 0.12	6.97	17.8	283.35	0.77	145.36
37	296.31396	-14.97089	500	1.55 ± 0.12	6.52	15.9	294.40	0.80	131.66
38	296.20490	-14.75966	250	1.37 ± 0.10	5.74	11.6	260.40	0.97	101.32
39	296.23492	-14.72453	95	0.80 ± 0.06	7.49	15.1	152.41	0.97	128.27
40	296.23090	-14.75460	500	1.10 ± 0.09	7.59	18.2	209.69	0.82	148.76
41	296.23541	-14.73430	500	1.16 ± 0.09	6.20	12.4	219.38	0.98	107.88
42	296.19272	-14.86216	500	1.44 ± 0.11	6.14	13.6	273.66	0.89	115.82
43	296.24420	-14.73231	500	3.20 ± 0.25	4.89	12.8	607.40	0.75	108.19
44	296.31229	-14.75217	500	1.31 ± 0.10	6.20	13.2	248.96	0.92	113.13
45	296.25198	-14.88950	500	1.93 ± 0.17	6.60	18.2	366.74	0.71	146.81
46	296.24365	-14.87206	500	1.52 ± 0.13	6.41	15.2	289.23	0.83	126.88
47	296.21973	-14.88315	250	0.25 ± 0.02	9.78	14.4	47.81	1.33	127.30

NOTE. — The assignment of an indicative maximum age (Col. 4) for each cluster is discussed in § 4.2. The estimation of the structural parameters of the clusters is described in detail in § 7.

described as fractal) in scales starting from the largest giant molecular cloud down to individual clumps and cores. Within this scheme, the cluster population of NGC 6822, as presented above, should represent one specific length-scale of a whole spectrum of stellar concentrations in this galaxy, and the detected clusters themselves are most probably members of larger structures. In this section we uncover the complete structural spectrum of stellar clustering and quantify the hierarchical distribution of the blue stars in NGC 6822 with $\tau \lesssim 500$ Myr, as they are selected in § 3.

8.1. Detection of stellar structures in NGC 6822

In order to search for stellar concentrations of various length-scales we apply again the NN density method, as described in § 4.1, for the 10th nearest neighbor (NN). The selection of the 10th NN is made for reasons of consistency with the detection of star clusters in the previous sections. Our tests showed that the application of the NN method for larger num-

ber of neighbors (e.g., 30 or 50) would ‘smooth’ the derived structures and unify many of them into single larger ones, losing the ability to detect any fine-structure in the spatial distribution of stars. For the identification of stellar structures of different densities we select different density thresholds in the application of the NN method. Specifically, apart from the 3σ detection applied in § 5 for the identification of the cluster population of the galaxy, we apply the method for the lower density thresholds of 1σ and 2σ above the average background density level to identify structures that correspond to lower stellar density enhancements. For the detection of concentrations that correspond to high stellar density we apply the NN method with higher (4σ and 5σ) density threshold above the background level.

The stellar structures identified with the 10th NN density method are shown in the density contour map of Fig. 10. Isoleths of different colors indicate the structures derived

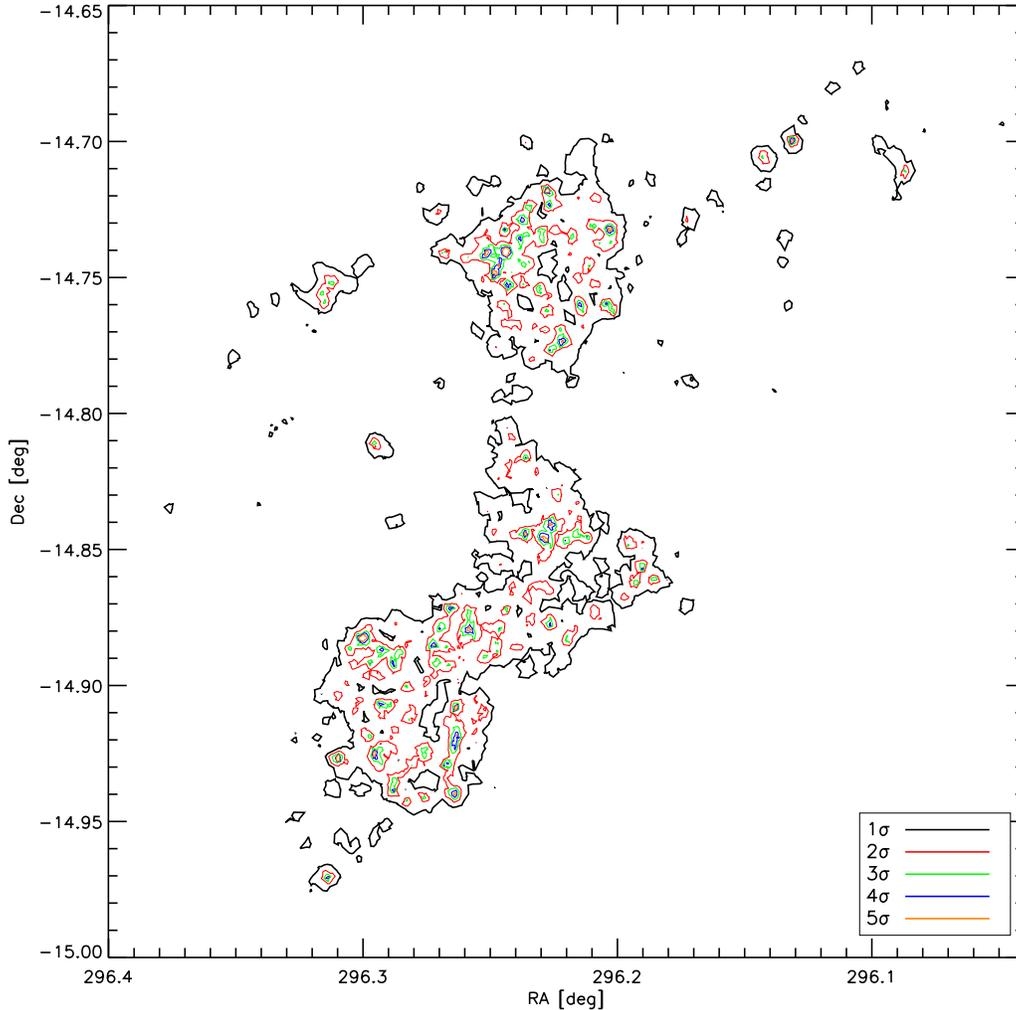


FIG. 10.— The density contour map constructed with the application of the 10th NN density method on our photometric data of NGC 6822. Isopleths within different density levels in σ , drawn with different colors, signify the corresponding identified stellar structures in the galaxy. All statistically important stellar structures are detected only in the main part of NGC 6822 disk. Therefore, the drawn contour map covers only this part of the galaxy instead of the whole observed field-of-view for reasons of clarity.

with the application of the method for different detection density thresholds. The cluster population of the 3σ detection is shown with green contours. This map is constrained to the main part of the galaxy, where all significant stellar concentrations, including its clusters, appear and which is known to host star formation (Cannon et al. 2006). From the map of Fig. 10 it can be seen that the low density threshold detections reveal large stellar structures, while the application of the method for higher density thresholds give rise to smaller and more compact stellar concentrations, which are actually located *in* the larger structures of the galaxy. This combination of high-density enhancements that correspond to small stellar systems and aggregates with low-density concentrations that represent large structures and stellar complexes is a clear signpost of hierarchical structure (Elmegreen 2010).

8.2. Dendrograms

An intuitive way to illustrate hierarchical structures is through the so-called *dendrograms*, introduced as “structure trees” for the analysis of molecular cloud structure by Houlahan & Scalo (1992), refined by Rosolowsky et al. (2008). A dendrogram is constructed by cutting the im-

age at different thresholds and identifying connected areas, while keeping track of the connection to “parent structures” (on a lower level) and “child structures” (on the next higher level, lying within the boundaries of its parent). A geometrically perfect hierarchy would be represented by a dendrogram where each parent branches out into the same number of children at each level.

We construct the dendrogram of the stellar structures detected in NGC 6822 with the NN density method for the various density thresholds considered, i.e., 1 to 5σ above the background density. In this dendrogram, shown in Fig. 11, the structures found at each density level are represented not only by the ‘leaves’ that end at the particular level, but by all branches present at that level. For example, at the 3σ level, there are 47 branches of the dendrogram (regardless whether they end here, continue to a higher level, or split into two or more branches), corresponding to the 47 detected stellar clusters. This dendrogram demonstrates that, while there are few centrally concentrated structures with a single peak, most structures split up into several substructures over at least three levels. The combination of this dendrogram with the contour map of Fig. 10 illustrates graphically the hierarchical spatial

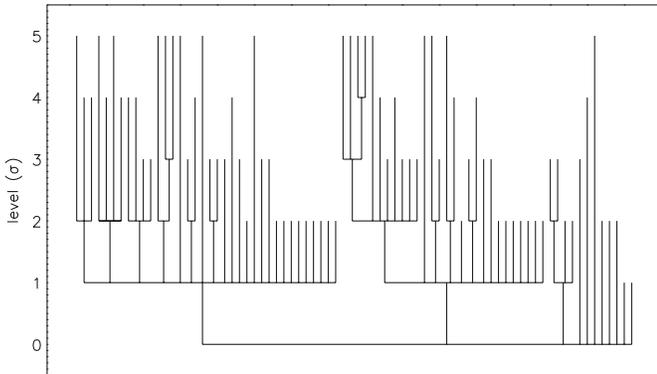


FIG. 11.— Dendrogram of the stellar structures identified at different levels in the 10th NN density map (Fig. 10), illustrating the hierarchical behavior of the clustering of the blue MS stars.

distribution of stars younger than 500 Myr in NGC 6822.

In the lower detection density threshold of 1σ (black isopleths in Fig. 10) there are few structures revealed, three of them being major stellar concentrations that qualify as large *stellar complexes*. These structures comprise a number of smaller *multiple* concentrations seen in the 2σ red isopleths of Fig. 10, which most probably correspond to the so-called *stellar aggregates* of the galaxy. The detected clusters (green 3σ isopleths) are actually members of these aggregates, fulfilling the typical image of hierarchical structuring of stars in a galaxy-scale. Higher density (4 and 5σ) detections correspond to the condensed stellar density peaks, which are seen to be the most compact centers of the larger structures.

8.3. Quantification of hierarchy

Another popular method in studies of hierarchical clustering is the *Minimum Spanning Tree* (MST) method, which may be applied with different cutoff lengths for the detection of different length-scales (e.g., Bastian et al. 2007, 2009). The MST method is excellent in quantifying the hierarchy in the discovered structures through the so-called Q parameter (see e.g., Cartwright & Whitworth 2004; Schmeja & Klessen 2006). It allows to distinguish between clusters with a central density concentration and hierarchical stellar concentrations with possible fractal substructure. Large Q values ($Q > 0.8$) describe centrally condensed clusters having a volume density $n(r) \propto r^{-\alpha}$, while small Q values ($Q < 0.8$) indicate concentrations with fractal substructure. Q is correlated with the radial density exponent α for $Q > 0.8$ and anti-correlated with the fractal dimension D for $Q < 0.8$. We determine Q for all structures detected at all levels with more than 45 members, since for poorer concentrations the method becomes unreliable due to increasing errors. Recent simulations of artificial clusters have shown that for clusters with $N \leq 45$ members, the expected error in the determination of the Q parameter is of the order of less than 0.05 (Schmeja 2010). Q varies systematically for structures showing a more elongated shape (Cartwright & Whitworth 2009; Bastian et al. 2009), therefore we apply the correction suggested by Bastian et al. (2009) when necessary.

The Q values for the structures detected at 1, 2, and 3σ density thresholds are all but one in the hierarchical regime ($Q < 0.8$), reaching Q values as low as $Q = 0.55$, corresponding to a fractal dimension of $D \approx 1.8$. The detections at higher density thresholds did not provide stellar structures rich enough to allow such an analysis. The Q values for the five 1σ structures with more than 45 stellar members range

from 0.56 to 0.73, and those for the ten 2σ structures from 0.55 to 0.83. There are only two clusters detected in the 3σ density threshold that include more than 45 stars, clusters No. 1 and 2 in Table 1. They are also found to be hierarchically structured with values of $Q = 0.62$ and 0.77 respectively. The average Q value for the structures revealed in all three density levels give evidence of fractal concentrations with $\bar{Q} = 0.70$. This value demonstrates the hierarchical nature of the clustering in NGC 6822. All but one of the analyzed structures are classified as hierarchical, i.e., they have significant (possible fractal) substructure rather than a smooth density gradient. It should be noted that the numbers of stars in the objects revealed at density levels with thresholds $\geq 3\sigma$ are too low to permit a meaningful Q analysis, but taking as example the two star clusters, for which this analysis was possible, most – if not all – of the 3σ clusters should be expected in the hierarchical regime as well.

Nevertheless, the unusual distribution of blue stars in the central part of NGC 6822 and their apparent hierarchy may be the result of differential extinction. For example, the two vacant areas to the east and west of the central S-shaped distribution of blue stars (Fig. 10), may be caused by high levels of extinction. Indeed, a comparison of the spatial distribution of the cool component of neutral hydrogen with that of the blue stars shows an anticorrelation on large scales (dBW06, their Fig. 7). However, while this extinction seems to affect the large-scale stellar distribution (at 1σ density level), giving it the S-shape, it does not seem to affect the hierarchical distribution of smaller stellar structures detected in higher density levels (2 and 3σ). Concerning the smallest detected structures (at 4 and 5σ), the resolution of the available observations of the ISM in NGC 6822 does not allow the detection of any patchy extinction in smaller scales. As such, we cannot assess how small-scale differential extinction may affect the apparent hierarchy of stellar structures, and therefore we certainly cannot exclude it as a possible bias.

In this case the derived Q values would indicate that the stars were in fact not in total hierarchically spread. It is also worth noting that if the largest stellar structures, shown in Fig. 10, are approximately 2D (i.e., much longer and wider than deep) the Q values returned by the MST method should be interpreted differently, since the crossover between ‘fractal’ and ‘centrally concentrated’ in the 2D case becomes 0.72 (see, Bastian et al. 2009), and thus the structures may be found to be less hierarchical.

8.4. Correlation of number of stars and radii

The correlation between the number of stars and radius seen for the clusters of NGC 6822 detected at the 3σ level (§ 7.1) is also observed for the structures we identify with the application of the NN method with different detection levels. This correlation is shown in Fig. 12 for detections with density thresholds of 1, 2, 4 and 5σ . The number of stars correlates with the radii of the structures with about the same slope of $k \approx 0.53$. Only the 5σ structures show a different behavior, but this plot suffers from the small number of objects. Adams et al. (2006) found a slope of $k = 0.54$ for young Galactic clusters, very close to the slope we find for the detected stellar structures and clusters in NGC 6822. As pointed out by Allen et al. (2007), these results are similar to that of Larson’s relations for molecular clouds, $\rho \sim R^{-1}$ (Larson 1981), implying a constant column density of the gas in molecular clouds.

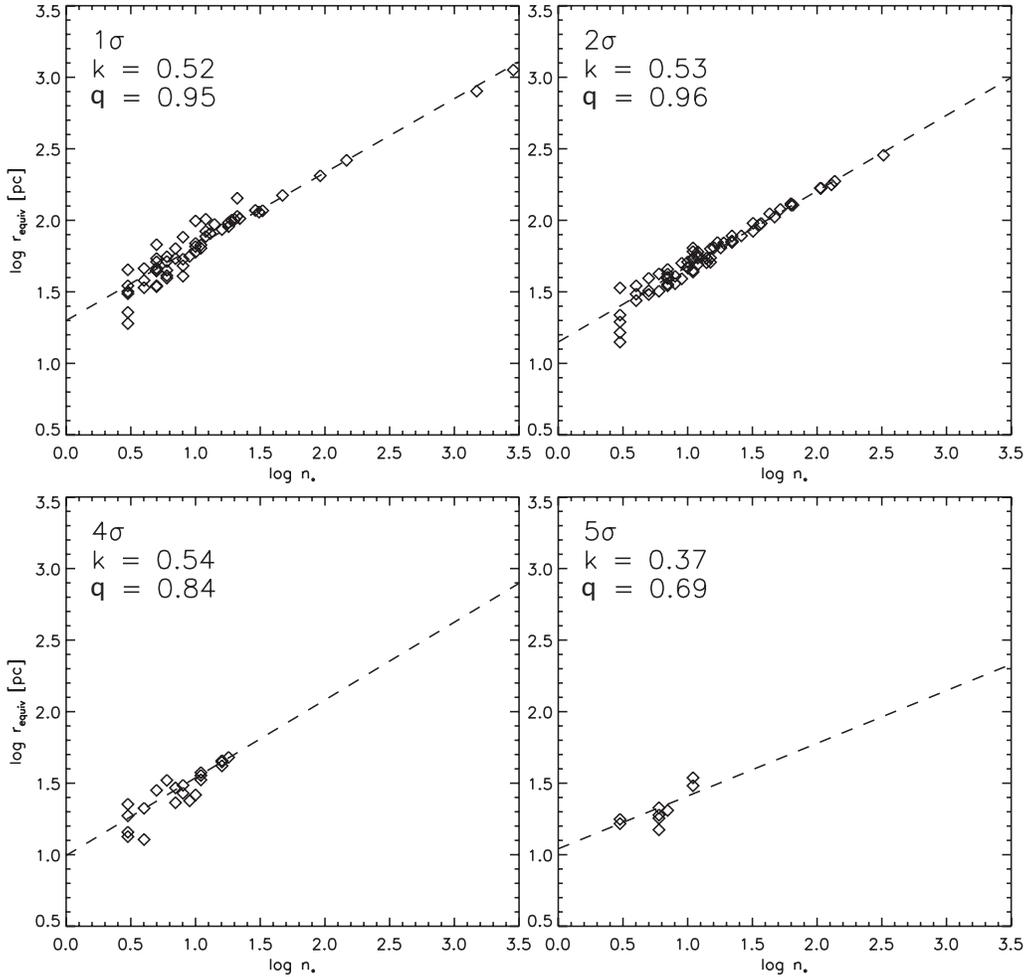


FIG. 12.— Correlation between the number of detected stars and r_{equiv} for the stellar structures of NGC 6822 identified with the NN method for various density detection levels. The corresponding slopes, k , and correlation coefficients, q , are also given. This correlation is similar to that we find for cluster population of the galaxy (§ 7.1) and consistent with findings for Galactic clusters (see § 7.1).

8.5. Current Star formation in NGC 6822

Cannon et al. (2006) performed *Spitzer* Space Telescope imaging of NGC 6822 and combined it with $H\alpha$, HI and radio continuum observations to study the nature of the emission in these wavebands on spatial scales of ~ 130 pc. They found strong variations in the relative ratios of $H\alpha$ and IR flux throughout the central disk of the galaxy, and that the localized ratios of dust to HI gas are about a factor of 5 higher than the global value of NGC 6822. These authors identified 16 IR emission complexes in the central part of the galaxy, six of which correspond to detections in the radio continuum image. The major HII regions, i.e., the strongest $H\alpha$ sources of the galaxy are also luminous in the IR and identified among the IR emission complexes, but in general $H\alpha$ and IR emission are not always cospatial. The HI distribution in the same area contains mostly high surface brightness (column densities $\gtrsim 10^{21}$ cm $^{-2}$), and it is clumpy with dense combs of neutral gas surrounding various emission peaks in other wavebands.

It is worthwhile to compare the star-forming complexes identified by Cannon et al. (2006) with the structures revealed from our study. The IR emission complexes are indicated by circles in Fig. 13, overlaid on our NN density map of the central part of NGC 6822 disk. This map appears more smooth than those shown before because we constructed it by apply-

ing the NN density method for the more gross number of the 50th NN, in order to achieve an angular resolution comparable to that provided by the nebular and dust emission observations. The comparison of our stellar structures with the IR-bright regions of Cannon et al. on the map of Fig. 13 shows a correlation of the stellar density peaks with the maximum IR emission only in the northern part of the galaxy, in particular, their regions 9 and 10 coincide with peaks in the stellar density. In the southern part they are significantly displaced from each other. Here, current star formation takes place at the western rim of the region of high stellar density. This is reminiscent of the spatial distribution of stellar birth in spiral arms or tidal tails, and points towards an external interaction (see also Karamelas et al. 2009). On the other hand, this spatial disagreement between peaks in IR emission and in stellar density in the southern central region of NGC 6822 may simply suggest that young stars are not yet revealed in their natal clusters, and we only detect the most evolved stellar concentrations in this part of the galaxy.

9. DISCUSSION AND CONCLUSIVE REMARKS

The formation of stars and star clusters in the interstellar matter (ISM) is controlled by the complex dynamical interplay between self-gravity and supersonic turbulence (Mac Low & Klessen 2004). On large scales, the turbulent motions in the ISM are highly supersonic with Mach numbers

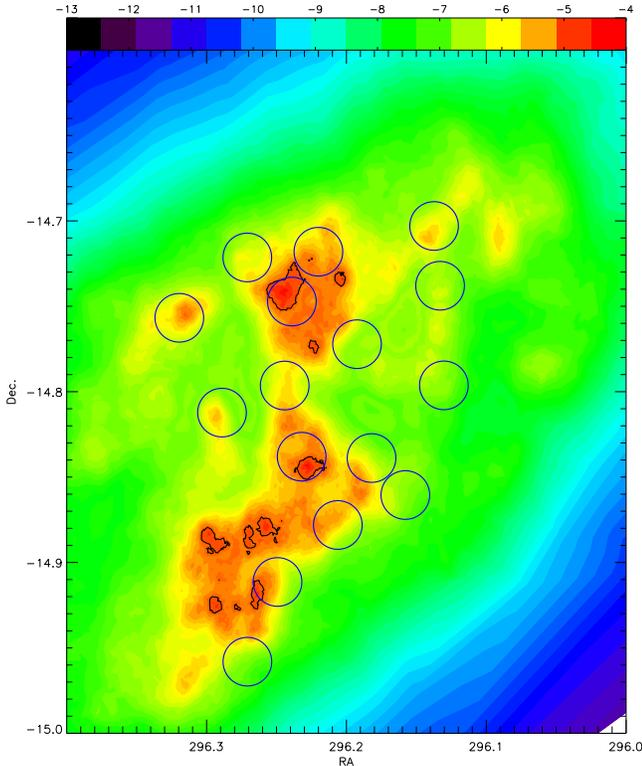


FIG. 13.— The 50th NN density map of the blue MS stars in the central region of NGC 6822 (in logarithmic scale) with blue circles overlaid indicating the IR-bright complexes identified by Cannon et al. (2006) with *Spitzer*.

up to several tens in giant molecular clouds. On scales of individual star-forming cloud cores, the turbulent velocity field becomes subsonic, with a well-defined power-law connecting these scales (Larson 1981) which could be the result of the scale-free nature of the turbulent cascade (Elmegreen & Scalo 2004; Scalo & Elmegreen 2004). The resulting morphological structure has often been interpreted in terms of hierarchical fractals (e.g., Elmegreen & Falgarone 1996; Stutzki et al. 1998; see also Federrath et al. 2009, 2010).

Turbulence plays a dual role. On global scales it provides support, while at the same time it can promote collapse locally. It creates strong density fluctuations with gravity taking over in the densest and most massive regions, where collapse sets in to build up individual stars (Klessen 2001a). Together with the thermodynamic properties of the gas and magnetic fields this regulates the fragmentation behavior in star forming clouds. The properties of young star clusters are thus directly related to the statistical characteristics of the underlying turbulence in the star-forming gas (Ballesteros-Paredes et al. 2007). This holds for the stellar IMF (Klessen & Burkert 2000, 2001; Hennebelle & Chabrier 2008, 2009), the protostellar accretion rates (Klessen 2001b; Schmeja & Klessen 2004), the star-formation efficiency and timescale (Klessen et al. 2000; Heitsch et al. 2001; Vázquez-Semadeni et al. 2003; Krumholz & McKee 2005), or the question of when and where dense clusters with high-mass stars form and when and where to expect a more distributed population of lower-mass stars (e.g., Vázquez-Semadeni et al. 2009).

Quite a number of different measures have been proposed to support and statistically characterize the link be-

tween the morphological and kinematical structure of the ISM and the population of star clusters that form in it. Efremov & Elmegreen (1998) find a correlation between the separation of stars and star clusters and their age, and interpret that result in terms of the linewidth-size relation in the ISM first discussed by Larson (1981). As velocity and size converts into a timescale, they conclude that the formation of molecular clouds and stellar birth in their interior proceeds on timescales of a few turbulent crossing times (Elmegreen et al. 2000; Elmegreen 2007) (see also Ballesteros-Paredes et al. 1999; Hartmann et al. 2001; Glover et al. 2010) which is a signpost of star formation controlled by interstellar turbulence (Elmegreen & Efremov 1997; Mac Low & Klessen 2004). Further evidence is provided by the fact that the mass spectrum of molecular clouds and clumps within the clouds follows a power law, $dN/dM \propto M^{-\alpha}$, with an exponent in the range $1.5 \lesssim \alpha \lesssim 2.0$ (Stutzki & Guesten 1990; Williams et al. 1994; Kramer et al. 1998) which is very similar to the mass spectra of young star clusters as discussed in § 6. The value of $\alpha = 1.5 \pm 0.7$ that we derive for the young clusters in NGC 6822 is fully consistent with this picture.

As the ISM exhibits a very complex, hierarchical morphological structure, it stands to reason that stars follow a similar spatial pattern. We have studied that aspect in § 8 in terms of the distributions of blue stars in individual stellar structures. Using the 10th nearest neighbor map to identify clusters, we find that indeed these stars in NGC 6822 can be grouped into larger and larger aggregates in a hierarchical fashion when we vary the detection threshold. Similar results are found in the Magellanic Clouds (Gieles et al. 2008; Bastian et al. 2009; see also Hunter et al. 2003), M33 (Bastian et al. 2007), and M51 (Bastian et al. 2005). We note that the \mathcal{Q} -parameters derived for the individual star clusters in NGC 6822 indicate that the stars in the clusters themselves are hierarchically structured. It is a common feature of young star clusters that they reveal a high degree of sub-clustering when observed with sufficient resolution and sensitivity to identify individual stars down to the peak of the IMF (e.g., Cartwright & Whitworth 2004, 2008, 2009; Schmeja et al. 2008, 2009) with values that are consistent with numerical calculations of star-cluster formation (Schmeja & Klessen 2004). We conclude that we find direct evidence, that the blue stars in NGC 6822 exhibit a hierarchical spatial pattern from the scales of individual objects all the way up to the scale of the galaxy as a whole.

It is interesting to note in this context that when it is indeed true that the spatial distribution of stars and star clusters traces the statistical properties of ISM turbulence, then the absence of a clear break in the hierarchy could indicate that turbulence is driven on kpc-scales. Possible mechanisms are global gravitational instability (e.g., Li et al. 2005), the magneto-rotational instability (MRI) in the disk of NGC 6822 (Beck et al. 1996; Balbus & Hawley 1998; Piontek & Ostriker 2007), or the accretion of fresh gas through the halo in form of cold streams or gas-rich satellites (Santillán et al. 2007; Sancisi et al. 2008; Klessen & Hennebelle 2010). Indeed, the "Northwestern Cloud" clearly visible in Fig. 1 has been speculated to be a separate system, possibly interacting with NGC 6822 (de Blok & Walter 2000, 2003). This interaction could also be responsible for a possible increase of the star formation rate in the past 100 Myr (Hodge 1980; see however Gallart et al. 1996a, for a different opinion).

In this paper we present a thorough investigation of the cluster population with age $\lesssim 500$ Myr and the hierarchy in the spatial distribution of main-sequence stars of this age in the Local Group dwarf irregular galaxy NGC 6822. Our observational material comprises optical imaging from the 8.2-m SUBARU Telescope, providing the most complete point source catalog of the galaxy in terms of dynamic range and spatial coverage.

Star clusters are identified with the application of the Nearest-Neighbor (NN) density method for the 10th NN on the blue main-sequence stars in NGC 6822. Forty-seven distinct concentrations with ≥ 3 stellar members that are found with our method to have 10th NN density values 3σ above the average background density are identified as the star clusters of the galaxy. The physical dimensions, stellar density and limiting radii of the clusters are defined by this density limit. The size distribution of the detected clusters can be very well approximated by a Gaussian peaked at ~ 68 pc (with $\sigma \sim 18$ pc).

The total stellar masses of the clusters are estimated by extrapolation of the total observed stellar mass function of all clusters to the lower stellar masses, assuming that it has the shape of the average Galactic mass function (Kroupa 2002) down to $0.1 M_{\odot}$. The derived cluster masses resign in the range $10^3 - 10^4 M_{\odot}$. Their distribution follows very well a power-law with index $\sim -1.5 \pm 0.7$, somewhat shallower but consistent with the Cluster Initial Mass Function and the mass spectra found for clusters in other Local Group galaxies. Structural parameters, such as their Spitzer radius, the correspondent 3-dimensional stellar density and velocity dispersion, as well as their crossing and the two-body relaxation times are computed for the clusters from their total masses and stellar numbers. We find a correlation between the radii and stellar numbers of the detected clusters, which follows a power law similar to that found for Galactic embedded clusters.

We study the clustering behavior of the blue stars in the considered age-limit with the application of the NN density method and the detection of stellar structures in different density levels, other than 3σ used for the establishment of the clusters. We identify, thus, stellar concentrations of various length-scales, clusters being the representative of one of them. High-density stellar structures are revealed from the application of the NN method with higher (4σ and 5σ) density threshold above the average density level, while the larger loose stellar structures, which include the denser ones, are recognized by the application of the method for lower (1σ and 2σ) density thresholds. All significant stellar concentrations, including the clusters, appear in the main (star-forming) part of the galaxy. The density maps constructed with this technique provide clear indications of hierarchically structured stellar concentrations in NGC 6822, in the sense that small dense stellar concentrations are located *inside* larger and looser ones. We illustrate this hierarchy by the so-called *dendrogram*, or structure tree of the detected stellar structures in NGC 6822, which demonstrates that most of the detected structures split up into several substructures over at least three levels.

The majority of the detected star clusters in NGC 6822 has ages between 250 and 500 Myr, which is longer than the crossing time of the galaxy, the timescale on which hierarchical cluster distributions in the LMC and SMC are erased (e.g., Bastian et al. 2009). As a consequence, the finding that these

clusters have preserved their structure is in itself very interesting. However, our catalog of “stellar clusters” comprises large stellar groups with sizes larger than the typical pc-scale Galactic clusters; the smallest cluster in our catalog is about 20 pc in size. As such, their large sizes is a possible explanation why these clusters have preserved their structure longer than one crossing time of the galaxy.

We quantify the hierarchy of these structures with the use of the Minimum Spanning Tree method and the Q parameter. We find that the Q values for the structures detected at 1 , 2 , and 3σ density thresholds reside in the hierarchical regime ($Q < 0.8$), reaching Q values that correspond to a fractal dimension of $D \approx 1.8$. The correlation between the number of stars and radius seen for the clusters of NGC 6822 is also observed for the larger stellar structures, identified at the 1σ and 2σ density levels, as well as for the smaller dense concentration identified at the 4σ density level. It is worth noting that some of the large high-density stellar concentrations, particularly in the northern part of the star-forming portion of the galaxy, coincide with IR-bright structures earlier identified with *Spitzer*, associated with high column density ($\gtrsim 10^{21} \text{ cm}^{-2}$) neutral gas, indicating structures that currently form stars.

The clusters of NGC 6822, which we identify at the 3σ density level of the NN method, are found to be themselves internally structured. Considering the ages of these clusters, this result is also interesting, because as found for small compact clusters, any substructure is expected to have been rapidly erased on very short time-scales (Allison et al. 2010). However, the clusters we detect in NGC 6822 are large stellar groups, which may have survived strong disruptions for periods of time longer than their crossing times. Previous simulations of fractal star clusters by Goodwin & Whitworth (2004) have shown that even an initially homogeneous cluster can develop substructure, if it is born with coherent velocity dispersion. As a consequence, the substructure we observe in our clusters may not be the present exhibition of their original ‘primordial’ substructure, but one induced later. The same authors find that the velocity dispersion is a key parameter, determining the survival of substructure, which can last for several crossing times. Therefore, it is possible that at least some of our clusters may have sustained their initial substructure. In favor to this, spatial substructure has been identified in open clusters of the Milky Way as old as ~ 100 Myr (Sánchez & Alfaro 2009).

The morphological structure of the stellar concentrations we identified in NGC 6822 resembles the structural behavior of the interstellar matter, which in principal is *hierarchical* and *dominated by turbulent motions*. As such, this coincidence between the clustering of stars and the hierarchical structure of the ISM, as it is demonstrated in the present study, suggests that turbulence may play the major role in regulating clustered star formation in NGC 6822 on pc- and kpc-scales.

D.A.G. acknowledges financial support from the German Research Foundation (Deutsche Forschungsgemeinschaft, DFG) through grant GO 1659/1-2 and the German Aerospace Center (Deutsche Zentrum für Luft- und Raumfahrt, DLR) through grant 50 OR 0908. S.S. acknowledges the support of the German Research Foundation through grants SCHM 2490/1-1 and KL 1358/5-2.

REFERENCES

- Adams, F. C., Proszkow, E. M., Fatuzzo, M., & Myers, P. C. 2006, *ApJ*, 641, 504
- Allison, R. J., Goodwin, S. P., Parker, R. J., Portegies Zwart, S. F., & de Grijs, R. 2010, *MNRAS*, 1188 (arXiv:1004.5244)
- Allen, L., Megeath, S. T., Gutermuth, R., et al. 2007, in *Protostars and Planets V*, eds. B. Reipurth, D. Jewitt, & K. Keil (Tucson: Univ. Arizona Press), 361
- Balbus, S. A., & Hawley, J. F. 1998, *Reviews of Modern Physics*, 70, 1
- Ballesteros-Paredes, J., Hartmann, L., & Vázquez-Semadeni, E. 1999, *ApJ*, 527, 285
- Ballesteros-Paredes, J., Klessen, R. S., Mac Low, M.-M., & Vázquez-Semadeni, E. 2007, *Protostars and Planets V*, 63
- Bastian, N., Gieles, M., Efremov, Y. N., & Lamers, H. J. G. L. M. 2005, *A&A*, 443, 79
- Bastian, N., Ercolano, B., Gieles, M., Rosolowsky, E., Scheepmaker, R. A., Gutermuth, R., & Efremov, Y. 2007, *MNRAS*, 379, 1302
- Bastian, N., Gieles, M., Ercolano, B., Gutermuth, R. 2009, *MNRAS*, 392, 868
- Bastian, N., Covey, K. R., & Meyer, M. R. 2010, *ARA&A* in press (arXiv:1001.2965)
- Battinelli, P., Demers, S., & Letarte, B. 2003, *A&A*, 405, 563
- Beck, R., Brandenburg, A., Moss, D., Shukurov, A., & Sokoloff, D. 1996, *ARA&A*, 34, 155
- Bik A., Lamers H. J. G. L. M., Bastian N., Panagia N., Romaniello M., 2003, *A&A*, 397, 473
- Cannon, J. M., et al. 2006, *ApJ*, 652, 1170
- Carpenter, J. M. 2000, *AJ*, 120, 3139
- Cartwright, A., & Whitworth, A. P. 2004, *MNRAS*, 348, 589
- Cartwright, A., & Whitworth, A. P. 2008, *MNRAS*, 390, 807
- Cartwright, A., & Whitworth, A. P. 2009, *MNRAS*, 392, 341
- Casertano, S., & Hut, P. 1985, *ApJ*, 298, 80
- Chabrier, G. 2003, *PASP*, 115, 763
- de Blok, W. J. G., & Walter, F. 2000, *ApJ*, 537, L95
- de Blok, W. J. G., & Walter, F. 2003, *MNRAS*, 341, L39
- de Blok, W. J. G., & Walter, F. 2006, *AJ*, 131, 343 (dbW06)
- de Grijs, R., & Anders, P. 2006, *MNRAS*, 366, 295
- de Grijs R., Goodwin S. P., 2008, *MNRAS*, 383, 1000
- de Grijs R., Anders P., Bastian N., Lynds R., Lamers H. J. G. L. M., O'Neil E. J., 2003, *MNRAS*, 343, 1285
- Efremov, I. N., Ivanov, G. R., & Nikolov, N. S. 1987, *Ap&SS*, 135, 119
- Efremov, Y. N., & Elmegreen, B. G. 1998, *MNRAS*, 299, 588
- Elmegreen, B. G. 2000, *ApJ*, 530, 277
- Elmegreen, B. G. 2007, *ApJ*, 668, 1064
- Elmegreen, B. G. 2010, *IAU Symposium*, 266, *Star clusters: basic galactic building blocks throughout time and space* ed. R. de Grijs & J. R. D. Lépine, (Cambridge: Cambridge Univ. Press), 3
- Elmegreen, B. G., & Falgarone, E. 1996, *ApJ*, 471, 816
- Elmegreen, B. G., & Efremov, Y. N. 1997, *ApJ*, 480, 235
- Elmegreen, B. G., & Scalo, J. 2004, *ARA&A*, 42, 211
- Elmegreen, B. G., Efremov, Y., Pudritz, R. E., & Zinnecker, H. 2000, in *Protostars and Planets IV*, eds. V. Mannings, A. P. Boss, & S. S. Russell (Tucson: Univ. Arizona Press), p. 179
- Federrath, C., Klessen, R. S., & Schmidt, W. 2009, *ApJ*, 692, 364
- Federrath, C., Roman-Duval, J., Klessen, R. S., Schmidt, W., & Mac Low, M.-M. 2010, *A&A*, 512, A81
- Gallart, C., Aparicio, A., Bertelli, G., & Chiosi, C. 1996a, *AJ*, 112, 1950
- Gallart, C., Aparicio, A., Bertelli, G., & Chiosi, C. 1996b, *AJ*, 112, 2596
- Gieles, M., Bastian, N., & Ercolano, B. 2008, *MNRAS*, 391, L93
- Gieles, M. 2009, *MNRAS*, 394, 2113
- Girardi, L., Bertelli, G., Bressan, A., Chiosi, C., Groenewegen, M. A. T., Marigo, P., Salasnich, B., & Weiss, A. 2002, *A&A*, 391, 195
- Glover, S. C. O., Federrath, C., Mac Low, M.-M., & Klessen, R. S. 2010, *MNRAS*, 404, 2
- Goodwin, S. P., & Whitworth, A. P. 2004, *A&A*, 413, 929
- Gouliermis, D., Keller, S. C., de Boer, K. S., Kontizas, M., & Kontizas, E. 2002, *A&A*, 381, 862
- Gouliermis, D., Kontizas, M., Kontizas, E., & Korakitis, R. 2003, *A&A*, 405, 111
- Gouliermis, D. A., 2010, in *Star-forming dwarf galaxies: following Ariadne's thread in the cosmic labyrinth*, *Physica Scripta*, in press
- Hartmann, L., Ballesteros-Paredes, J., & Bergin, E. A. 2001, *ApJ*, 562, 852
- Heitsch, F., Mac Low, M.-M., & Klessen, R. S. 2001, *ApJ*, 547, 280
- Hennebelle, P., & Chabrier, G. 2008, *ApJ*, 684, 395
- Hennebelle, P., & Chabrier, G. 2009, *ApJ*, 702, 1428
- Hodge, P.W., 1980, *ApJ*, 241, 125
- Houllahan, P., & Scalo, J. 1992, *ApJ*, 393, 172
- Hunter, D. A., & Elmegreen, B. G. 2004, *AJ*, 128, 2170
- Hunter, D. A., Elmegreen, B. G., Dupuy, T. J., Mortonson, M. 2003, *AJ*, 126, 1836
- Israel, F.P., Bontekoe, Tj.R., Kester, D.J.M, 1996, *A&A*, 308, 723
- Ivanov, G. R. 1996, *A&A*, 305, 708
- Karamelas, A., Dapergolas, A., Kontizas, E., Livanou, E., Kontizas, M., Bellas-Velidis, I., & Vílchez, J. M. 2009, *A&A*, 497, 703
- Klessen, R. S. 2001a, *ApJ*, 556, 837
- Klessen, R. S. 2001b, *ApJ*, 550, L77
- Klessen, R. S., & Burkert, A. 2000, *ApJS*, 128, 287
- Klessen, R. S., & Burkert, A. 2001, *ApJ*, 549, 386
- Klessen, R. S., & Hennebelle, P. 2010, *A&A* in press (arXiv:0912.0288)
- Klessen, R. S., Heitsch, F., & Mac Low, M.-M. 2000, *ApJ*, 535, 887
- Komiyama, Y., et al. 2003, *ApJ*, 590, L17
- Kramer, C., Alves, J., Lada, C., Lada, E., Sievers, A., Ungerechts, H., & Walmsley, M. 1998, *A&A*, 329, L33
- Kroupa, P. 2002, *Science*, 295, 82
- Kroupa, P. 2008, *Lecture Notes in Physics*, Berlin Springer Verlag, 760, 181
- Krumholz, M. R., & McKee, C. F. 2005, *ApJ*, 630, 250
- Lada, C. J., & Lada, E. A. 2003, *ARA&A*, 41, 57
- Larson, R. B. 1981, *MNRAS*, 194, 809
- Li, Y., Mac Low, M.-M., & Klessen, R. S. 2005, *ApJ*, 620, L19
- Mac Low, M.-M., & Klessen, R. S. 2004, *Reviews of Modern Physics*, 76, 125
- Mafiz Apellániz, J., & Úbeda, L. 2005, *ApJ*, 629, 873
- Massey, P. 2006, *The Local Group as an Astrophysical Laboratory*, 164
- Massey, P., Olsen, K. A. G., Hodge, P. W., Jacoby, G. H., McNeill, R. T., Smith, R. C., & Strong, S. B. 2007, *AJ*, 133, 2393
- Massey, P., Olsen, K. A. G., Hodge, P. W., Strong, S. B., Jacoby, G. H., Schlingman, W., & Smith, R. C. 2006, *AJ*, 131, 2478
- Mateo, M.L. 1998, *ARA&A*, 36, 435
- McCraday N., Graham J. R., 2007, *ApJ*, 663, 844
- Miller, G. E., & Scalo, J. M. 1979, *ApJS*, 41, 513
- Miyazaki, S., et al. 2002, *PASJ*, 54, 833
- Piontek, R. A., & Ostriker, E. C. 2007, *ApJ*, 663, 183
- Román-Zúñiga, C. G., Elston, R., Ferreira, B., & Lada, E. A. 2008, *ApJ*, 672, 861
- Rosolowsky, E. W., Pineda, J. E., Kauffmann, J., & Goodman, A. A. 2008, *ApJ*, 679, 1338
- Salpeter, E. E. 1955, *ApJ*, 121, 161
- Sánchez, N., & Alfaro, E. J. 2009, *ApJ*, 696, 2086
- Sancisi, R., Fraternali, F., Oosterloo, T., & van der Hulst, T. 2008, *A&A Rev.*, 15, 189
- Santillán, A., Sánchez-Salcedo, F. J., & Franco, J. 2007, *ApJ*, 662, L19
- Scalo, J. 1986, *Fundam. Cosmic Phys.*, 11, 1
- Scalo, J. 1998, in *ASP Conf. Ser. 142, The Stellar Initial Mass Function (38th Herstmonceux Conf.)*, ed. G. Gilmore & D. Howell (San Francisco, CA: ASP), 201
- Scalo, J., & Elmegreen, B. G. 2004, *ARA&A*, 42, 275
- Schmeja, S., 2010, *Astron. Nachr.* accepted
- Schmeja, S., & Klessen, R. S. 2004, *A&A*, 419, 405
- Schmeja, S., & Klessen, R. S. 2006, *A&A*, 449, 151
- Schmeja, S., Kumar, M. S. N., & Ferreira, B. 2008, *MNRAS*, 389, 1209
- Schmeja, S., Gouliermis, D. A., & Klessen, R. S. 2009, *ApJ*, 694, 367
- Skillman, E.D., Terlevich, R., Melnick, J. 1989, *MNRAS*, 240, 563
- Spitzer, L. 1987, Princeton, NJ, Princeton University Press, 1987, 191 p.
- Spitzer, L., Jr. 1958, *ApJ*, 127, 17
- Spitzer, L., Jr. 1969, *ApJ*, 158, L139
- Stutzki, J., & Guesten, R. 1990, *ApJ*, 356, 513
- Stutzki, J., Bensch, F., Heithausen, A., Ossenkopf, V., & Zielinsky, M. 1998, *A&A*, 336, 697
- van den Bergh, S. 2000, *Cambridge Astrophysics Series*, 35,
- Vázquez-Semadeni, E., Ballesteros-Paredes, J., & Klessen, R. S. 2003, *ApJ*, 585, L131
- Vázquez-Semadeni, E., Gómez, G. C., Jappsen, A.-K., Ballesteros-Paredes, J., & Klessen, R. S. 2009, *ApJ*, 707, 1023
- von Hoerner, S. 1963, *ZAp*, 57, 47
- Weldrake, D. T. F., de Blok, W. J. G., & Walter, F. 2003, *MNRAS*, 340, 12
- Weisz, D. R., Skillman, E. D., Cannon, J. M., Dolphin, A. E., Kennicutt, R. C., Jr., Lee, J., & Walter, F. 2008, *ApJ*, 689, 160
- Williams, J. P., de Geus, E. J., & Blitz, L. 1994, *ApJ*, 428, 693
- Wyder, T. K. 2001, *AJ*, 122, 2490
- Zhang Q., Fall S. M., 1999, *ApJ*, 527, L81